WEATHER STUDIES (JAW   (U) NATIONAL CENTER FOR
ATMOSPHERIC RESEARCH BOULDER CO RESEARCH A
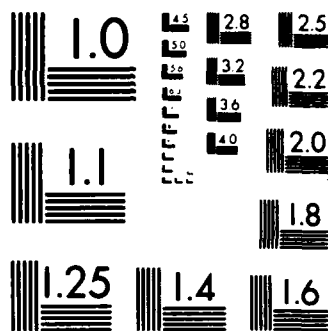
UNCLASSIFIED   M R HJELMFELT MAR 86 DOT/FAA/PM-86/22   F/G 4/2   NL

MICROCOPY RESOLUTION TEST CHART

NATIONAL BUREAU OF STANDARDS 1963 A

DOT/FAA/PM-86/22

Program Engineering
and Maintenance Service
Washington, D.C. 20591

AD-A184 827

The Microbursts of June 22,1982 in the Joint Airport Weather Studies (JAWS) Project

M. R. Hjelmfelt

Research Applications Program
National Center for Atmospheric Research
P.O. Box 3000
Boulder, CO 80307

March 1986

US. Department of Transportation

Federal Aviation Administration

87   9 14   030

NOTICE

This document is disseminated under the sponsorship of the Department of Transportation in the interest of information exchange. The United States Government assumes no liability for its contents or use thereof.

1. Report No.	2. Government Accession No.	3. Recipient's Catalog No.
DOT/FAA/PM-86/22	ADA184827	

4. Title and Subtitle	5. Report Date
The Microbursts of June 22, 1982, in the Joint Airport Weather Studies (JAWS) Project	March 1986
	6. Performing Organization Code

	8. Performing Organization Report No.
7. Author's) Mark R. Hjelmfelt, Ph.D.	

9. Performing Organization Name and Address	10. Work Unit No. (TRAIS)
Research Applications Program National Center for Atmospheric Research P. O. Box 3000 Boulder, Colorado 80307	
	11. Contract or Grant No. DTFA01-82-Y-10513
	13. Type of Report and Period Covered

12. Sponsoring Agency Name and Address	
U.S. Department of Transportation Federal Aviation Administration Program Engineering and Maintenance Service Washington, D.C. 20590	Final Report
	14. Sponsoring Agency Code APM-310

16. Abstract

On June 22, 1982, a line of storms developed in the Joint Airport Weather Studies (JAWS) network near Denver, Colorado, in response to interaction of boundary-layer convergence lines and wind parallel lines of convection. These storms produced six microbursts and one microburst line. Single and multiple Doppler radar data and surface network data were used to describe the structure and life cycle of the microburst outflows and to examine potential forcing mechanisms.

The microburst outflows can be classified into three types: isolated, generally symmetric outflows; outflows embedded in strong low-level environmental flow which reveal their symmetric diverging outflow structure only when the mean flow is eliminated; and the microburst line. Some of the microbursts decayed by weakening; others grew to larger-scale, less intense outflows.

All of the microbursts were associated with descending high-reflectivity cores, many of which showed evidence of convergence and associated reflectivity decreases below cloud base. Most of the microbursts exhibited some rotation aloft. However, the relationship between the location of rotation and the downdraft was variable. Well-developed rotation also tended to be short-lived, and timing of the appearance of rotation during the microburst life cycle varied from case to case. Application of the downdraft model of Srivastava (1985) indicated that sufficient negative buoyancy could be produced by evaporation and precipitation loading to account for the magnitude of the observed microburst downdrafts. It is concluded that the microbursts on this day were predominantly driven by microphysical and related thermodynamic effects due to processes of precipitation loading and water phase change.

17. Key Words	18. Distribution Statement
Microbursts, Wind Shear, Weather Radar, Doppler Radar, Joint Airport Weather Studies, Cloud Dynamics	This document is available to the public through the National Technical Information Service, Springfield, Virginia 22161.

19. Security Classif. (of this report)	20. Security Classif. (of this page)	21. No. of Pages	22. Price
Unclassified	Unclassified	43	

Form DOT F 1700.7 (8-72)   Reproduction of completed page authorized

TABLE OF CONTENTS

iii

LIST OF FIGURES

LIST OF TABLES

ACRONYMS

AGL – Above Ground Level

GMT – Greenwich Mean Time

JAWS – Joint Airport Weather Studies

MDT – Mountain Daylight Time

NCAR – National Center for Atmospheric Research

NIMROD – Northern Illinois Meteorological Research on Downbursts

PAM – Portable Automated Mesonet

PROFS – Program for Regional Observing and Forecasting Services

RDSS – Research Data Support System

1. INTRODUCTION

On June 22, 1982, several large thunderstorms developed in the Denver metropolitan area, producing heavy rain, hail, and several microbursts. Between 1535 and 1624 MDT (all times are given in Mountain Daylight Time), six microbursts and one microburst line were produced by two lines of storms which developed within the project area of the Joint Airport Weather Studies (JAWS) (McCarthy et al., 1982). These microbursts were observed by Doppler radars and the Portable Automated Mesonet (PAM) meteorological surface network.

This paper describes the development of these storms and the microbursts they produced. The characteristics of the microbursts are described and the structure and life cycle of two examples are discussed with respect to the general character of JAWS microbursts, leading to a consideration of potential forcing mechanisms for these microbursts.

Fujita (1981) gave the name "microburst" to a downdraft that produces a sudden outflow of damaging horizontal winds at the surface with a horizontal extent between 0.4 and 4.0 km. Outflows on this scale were inferred from observations during the Thunderstorm Project (Byers and Braham, 1949) and were studied extensively in the Northern Illinois Meteorological Research on Downbursts (NIMROD) Program and during the JAWS Project (Fujita, 1981, 1985; McCarthy et al., 1982). Outflows of this scale have been shown to be particularly hazardous to aircraft when encountered at low altitude (Fujita and Byers, 1977; Elmore et al., 1986).

In JAWS, the microburst was defined in reference to Doppler radar observations of the diverging outflow near the surface. The differential Doppler velocity across the divergence center must be ≥ 10 m s^{-1} and the initial distance between maximum approaching and receding centers must be < 4 km (Wilson et al., 1984).

The JAWS Project was held in the Denver area during the spring and summer of 1982. The primary observing systems consisted of three Doppler radars operated by the National Center for Atmospheric Research (NCAR), one S-band radar (CP-2), and two C-band radars (CP-3 and CP-4). Surface weather data were provided by the NCAR PAM network of 27 observing stations (Brock and Govind, 1977), and a larger-scale network operated by the Program for Regional Observing and Forecasting Services (PROFS) (Pratte and Clark, 1983). The average station spacing was approximately 4 km for PAM and 25 km for the PROFS mesonet. PAM data were recorded every minute and PROFS data every 5 min. Special soundings were taken from the Denver National Weather Service rawinsonde site, and several instrumented aircraft participated.

The JAWS observing network was centered on Denver's Stapleton International Airport. Figure 1 shows the locations of the JAWS radars and the PAM stations. The JAWS radar network was specifically designed to collect high-resolution multiple Doppler radar and surface data to allow the structure of microburst outflows to be studied. The longest radar baseline was 28 km between CP-2 and CP-4. The distance between CP-2 and CP-3 was 18 km, and between CP-3 and CP-4, 14 km. Radar scanning was concentrated near
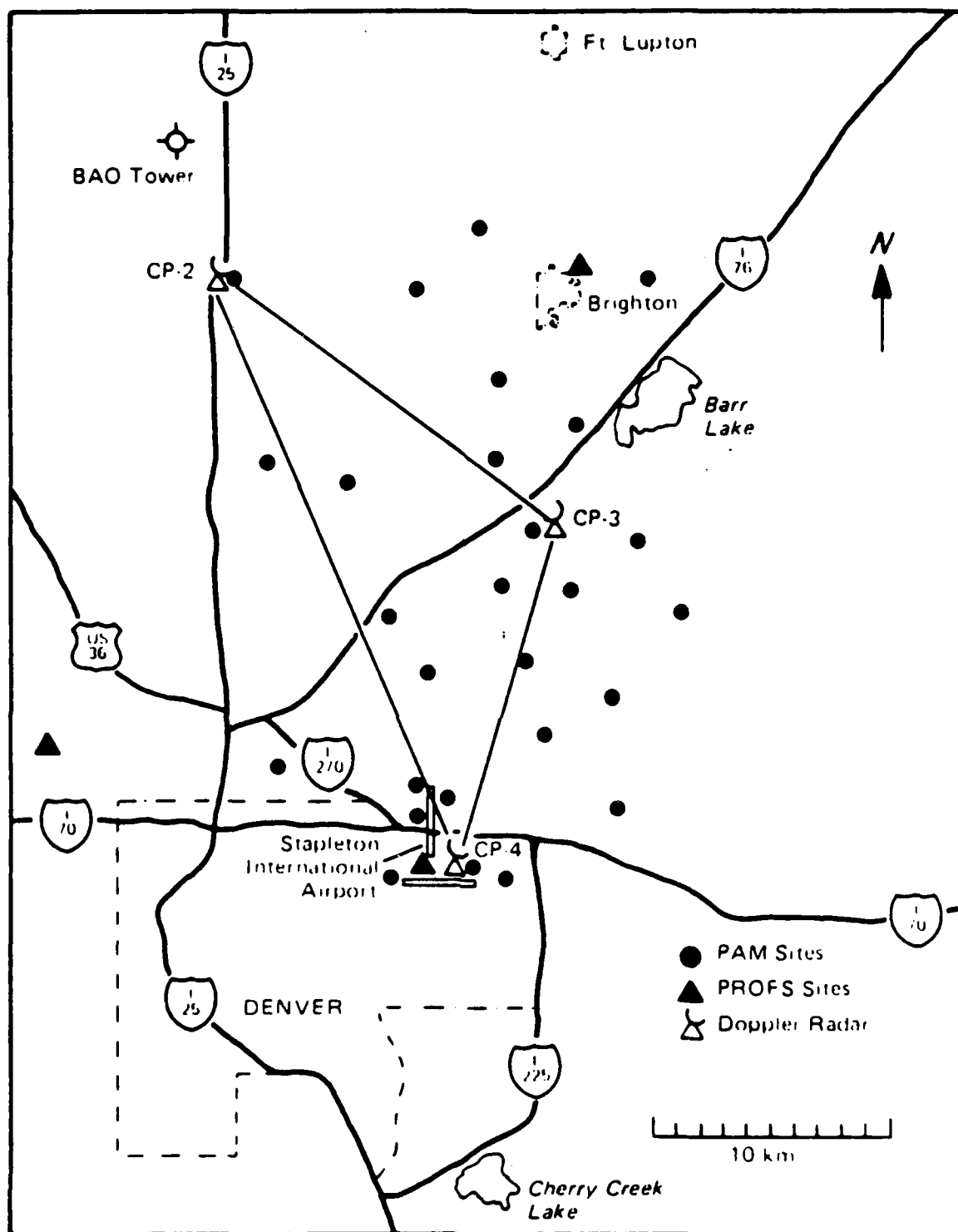
Figure 1. Map of the JAWS Project study area. PAM and PROFS surface networks and locations of Doppler radars are shown. (Radar triangle will be shown on subsequent figures for orientation.) Also shown is location of CP-4 radar at Stapleton International Airport.

2

the ground with lowest scans collecting data as near to the ground as possible. The lowest observed level was centered 30-120 m above the ground. Scanning strategy permitted new volume scans to begin every 2-2.5 min. McCarthy et al. (1983) give additional details about other facilities in the field experiment.

2. DATA ANALYSIS

The NCAR Research Doppler radars used in JAWS have nominal 1° half-power beam widths. In 1982, CP-2 had a minimum detectable signal of $\sim$ -18 dBZ at 25 km (-116 dBM). CP-3 and CP-4 had a signal of -5 dBZ at 25 km (-108 dBM) for typical dwell times of 5 x 10^{-3} sec. These radars have excellent detection capabilities for warm season, boundary-layer, optically-clear air.

On June 22, six microbursts and a microburst line were identified and examined. Microburst detection was based on observation of a diffluent velocity signature at low elevation by at least one Doppler radar. More events may have occurred than were identified, since the radars were not scanning all the time in all directions. It is also possible that there were some very small-scale (< 1 km) events which went undetected.

Wind fields were obtained from radial velocity data collected by all three Doppler radars with an over-determined (in a least-squares sense) dual-Doppler synthesis program developed at the National Severe Storms Laboratory (Kessinger et al., 1983; Wilson et al., 1984). Data editing was performed on NCAR's Research Data Support System (RDSS), which is an imaging, interactive computer system (Oye and Carbone, 1981). The vertical wind component was derived from an upward integration of the anelastic mass continuity equation. A zero vertical velocity lower boundary condition was assumed. Wind vectors were obtained on a grid with 300 m horizontal and 400 m vertical spacing, which is near the maximum resolution possible from the radars. The Cressman (1959) interpolation scheme (method of successive corrections) used an influence radius equal to the grid spacing.

These choices maximized the data resolution and provided a small amount of filtering. This analysis scheme is the same as that used by Wilson et al. (1984). A more detailed discussion of the analysis techniques and estimation of errors is contained in that paper. In this case, wind features with scales greater than about 2 km were well resolved, and useful information was obtained for scales down to 1 km.

PAM data were analyzed using a software package developed at NCAR. This analysis package permits interpolation of data onto a regular grid for analysis of derived fields such as divergence, vorticity, and equivalent potential temperature (Wilson and Carpenter, 1983).

3. SYNOPTIC SETTING

Surface observations at 0600 on June 22 indicated a decaying stationary front passing southeastward through the northeastern corner of Colorado. A high-pressure area, centered over Minnesota, extended into southcentral Nebraska. By 1200, the front had decayed sufficiently that no indication could be found in a regional surface analysis.

A 500 mb ridge extended southward through western Wyoming and the Utah-Colorado border at 0600. A short wave trough was expected to initiate convection over the eastern slopes of the Rockies and the Great Plains with stron· potential for thunderstorms.

3

The 0600 (1200 Greenwich Mean Time, GMT) Denver sounding, Fig. 2, exhibited potential instability sufficient for vigorous thunderstorms and small hail with a deep, dry sub-cloud layer expected. Winds were generally light (< 7 m s^{-1}) throughout the lower and middle troposphere, strengthening to 15 m s^{-1} above the tropopause. From this sounding the forecast Lifting Condensation Level was 600 mb (1.0° C at 2.8 km Above Ground Level, AGL), the convective temperature was 27° C, and the Lifted Index was calculated to be about 2.4.

By 1530, towering cumulus had formed between CP-3 and CP-4 along a developing boundary-layer convergence line passing through the JAWS network. The microbursts studied in this work were produced by these storms. The storms that initiated over the Rockies and moved out over the Plains, or developed over the Palmer Divide south of the study area and the Cheyenne Ridge to the north, will not be discussed.

4.   MESOANALYSIS

A narrow mesoscale line of convergence developed over the study area during the afternoon of June 22. Such convergence zones are common features of the summer afternoon boundary-layer airflow in the Denver area. Szoke et al. (1984) described one type of these features in their analysis of the June 3, 1981, Denver tornadoes. Recently, Abbs and Pielke (1986) have shown, by numerical simulations with a mesoscale model, that boundary-layer convergence lines may develop in the Denver area in the summer from topographic forcing. The importance of such boundaries to storm initiation has been discussed in Purdom and Marcus (1982) and Wilson and Schreiber (1986).

Early in the afternoon on June 22, the regional surface flow field indicated light winds with no coherent patterns and no indication of a convergence line. By 1520, the low-level flow began to become organized and a convergence line developed in the network.

Figure 3 shows the surface wind field and convergence line at 1520 using the combined PROFS and PAM surface mesonet works. The triangle in the figure indicates the Doppler radar network (see Fig. 1). The bold solid line indicates the location of the convergence line as observed by Doppler radar radial velocities and analysis of PAM network data. Only a weak temperature contrast was observed across the convergence line at this time ($\leq 1°$C). Lines of very weak echoes (generally < 0 dBZ) developed in the boundary layer aligned with the mean boundary-layer wind (presumably horizontal rolls). These are shown by the light dashed lines. Also at 1520, just to the southwest of CP-3, the first low-level precipitation echo (20 dBZ) from the microburst-producing storms appeared along the convergence line. This echo appeared near the intersection of the convergence line and the strongest wind parallel line. Convergence was strengthened as a gust front propagated through the network from large storms over the Palmer Divide to the south and a secondary surge strengthened the flow from the northwest (perhaps originating from mountain convection). Further convective development occurred as these interacted with the wind parallel lines and the existing convergence line.

Figure 4 shows the locations of the microbursts near the time of first observation of low-level divergence and their relation to low-level radar echoes and convergence lines. The microbursts formed within lines of echoes extending eastward across the low-level

4
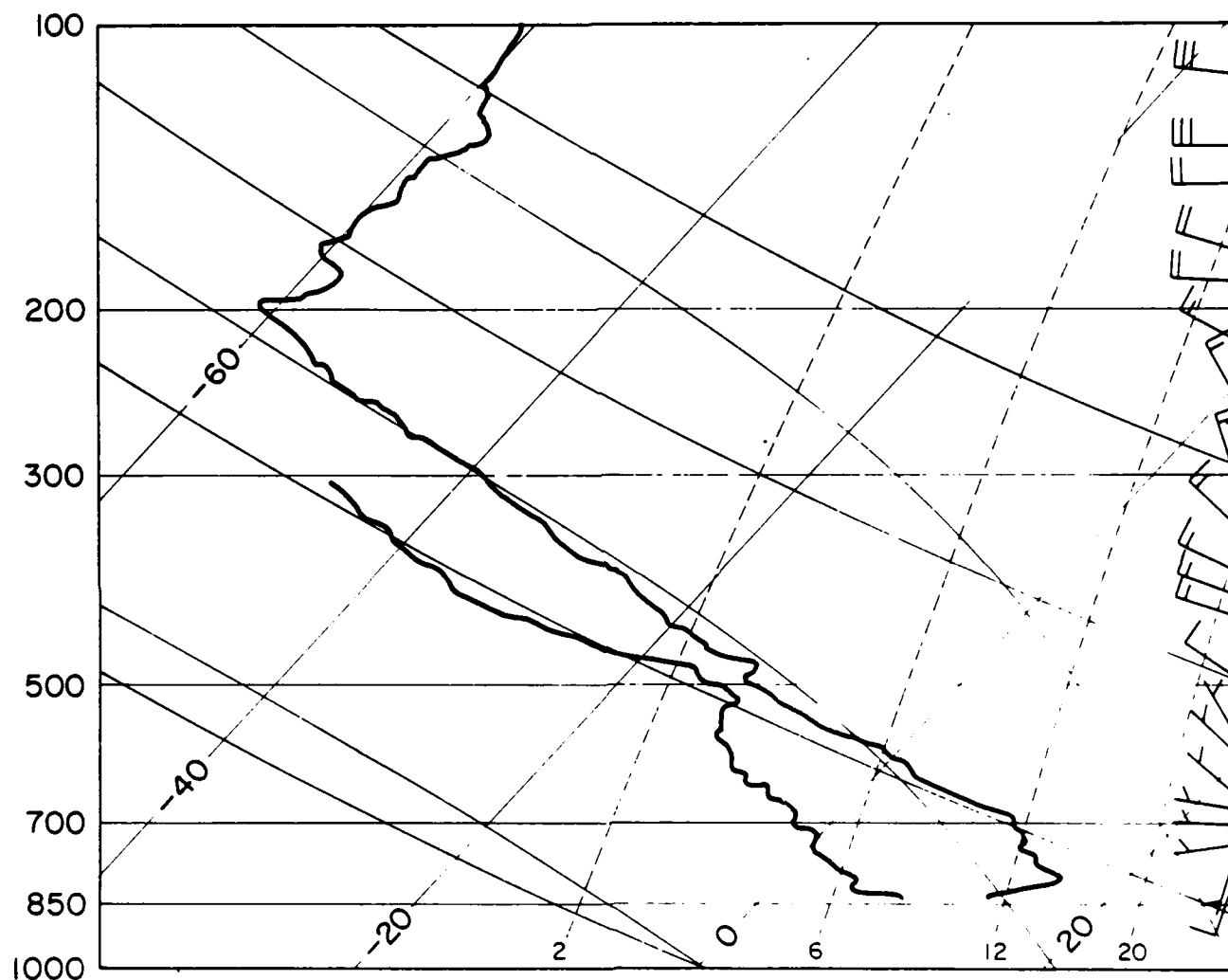
Figure 2. The 0600 MDT (1200 GMT) Denver sounding for June 22, 1982, plotted on a Skew-T Log-P diagram. Pressure is given in millibars. One full wind barb equals 5 m s^{-1}.
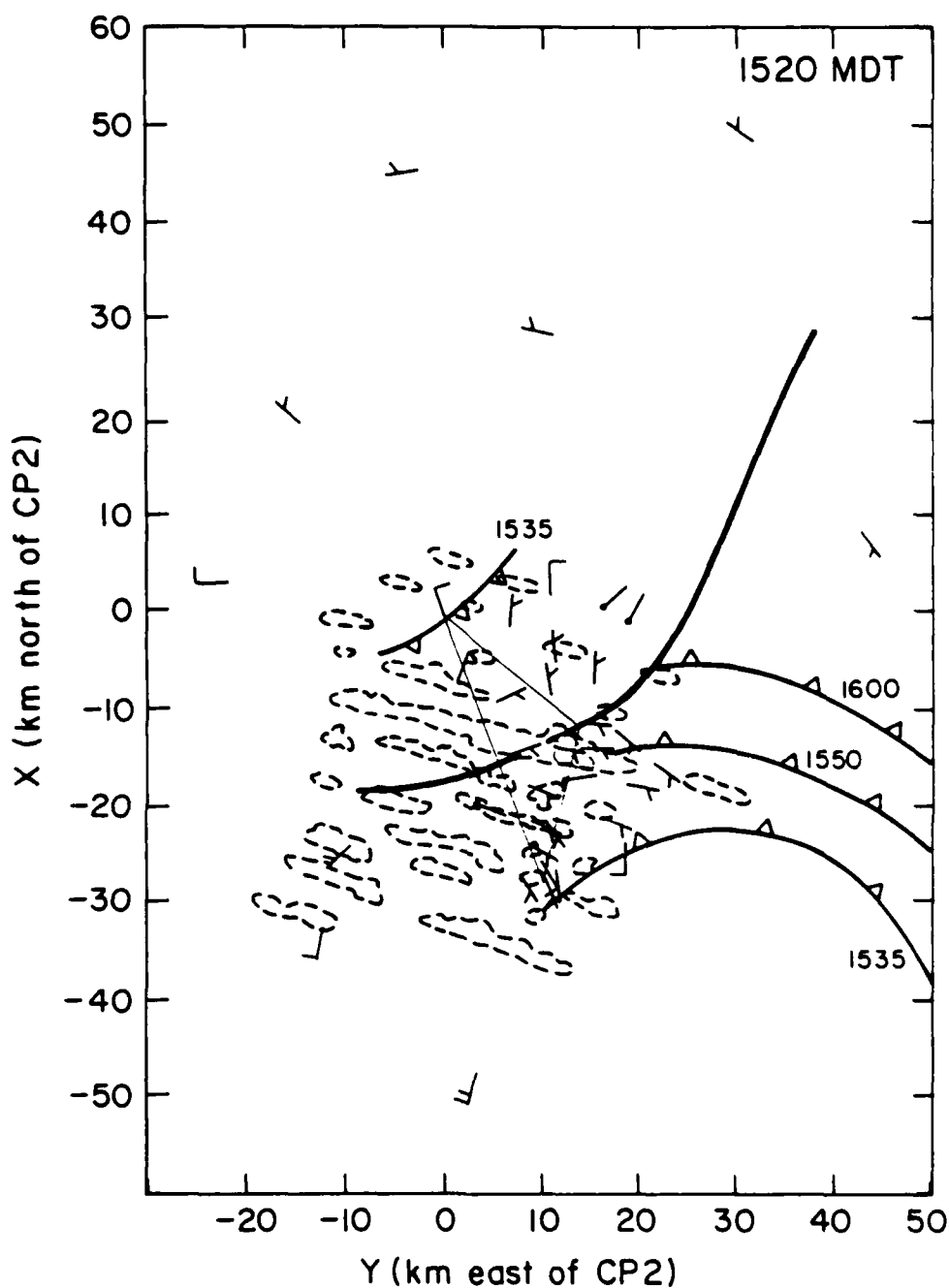
Figure 3. Mesoscale analysis for 1520 MDT: Wind observations from the PAM and PROFS networks; one full barb equals 5 m s^{-1}. Heavy solid line indicates estimated location of convergence line as observed by CP-2 and the surface networks. Solid lines indicate positions of gust front from storms to south and surge from northwest. Light dashed lines indicate lines of convection observed by CP-2 and CP-4 radars in the boundary layer (about 1513). Shaded area indicates first low-elevation radar echo > 10 dBZ. Triangle shows radar locations (see Fig. 1).
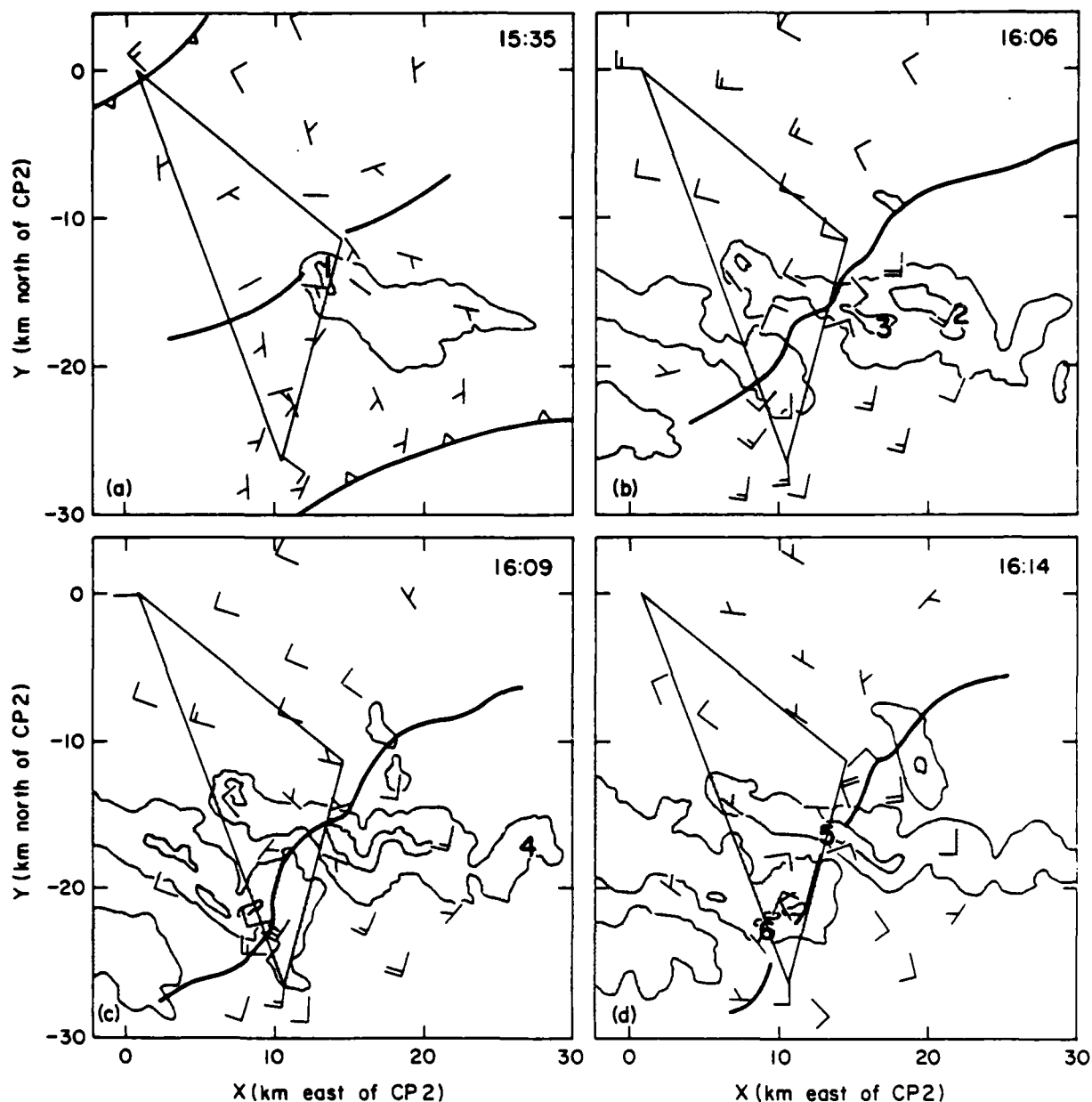
Figure 4. Relationship of microburst location to low-level radar echoes and convergence line. The convergence lines, as defined by Doppler radar observations, are given by solid lines. Low-level radar reflectivity is contoured for 25 and 50 dBZ, with echo area greater than 25 dBZ shaded. Microburst locations are shown as numbered, with the time of each panel chosen to coincide approximately with microburst outflow initiation: (a) 1535 MDT, (b) 1606 MDT, (c) 1609 MDT, and (d) 1614 MDT.

7

convergence line. A notable feature of these echoes is kinks (sharp bends and narrowings in the reflectivity pattern) between reflectivity cores. This is a common feature of lines of storms which produce microbursts, and is seen especially well in Fig. 4d.

Microburst 1 touched down at 1535 in a small area of > 55 dBZ echo (see Fig. 4a). A well-defined convergence line can be seen in the surface wind field and Doppler radial velocities; a composite estimate of its location is shown by the heavy dark line. Microburst 1 occurred very near this line. The locations of the gust front to the south and the estimated position of the secondary surge to the northwest are given by the light solid lines.

Microbursts 2, 3, and 4 also occurred in heavy precipitation cores, but did not occur along the convergence line (see Figs. 4b and 4c). Further development of the storms into long lines crossing the convergence line and intensification of the low-level convergence is also visible in these figures. By 1606 (Fig. 4b), the gust front and secondary surges had both reached the convergence line, resulting in greatly increased shear. Doppler radar observations indicate that the convergence line extended to an altitude of 1–1.5 km. Wind speed differentials across the line in excess of 15 m s^{-1} were measured by PAM, and peak convergence calculated from multiple Doppler analysis exceeded -10^{-2}s^{-1}.

Figure 4d shows the low-level wind field at 1614. By this time, lines of thunderstorms had developed across the network and three microbursts were occurring in the area. Despite these complications, the convergence line is still well defined. Microbursts 5 and 6 had just touched down along the convergence line. Microburst 6 eventually became a part of a large microburst line, which extended roughly east-northeast through the location of Microburst 6, and destroyed the convergence line (see Section 6.4).

On this day, observations suggest that deep convection developed in response to the interaction of boundary-layer convergence lines and wind parallel lines of convection in the boundary layer. The relationship of the boundary layer convergence to the microbursts is less clear. Microbursts 1, 5, and 6 touched down close to the resulting convergence line. Microbursts 2, 3, and 4, on the other hand, touched down some distance away in separate reflectivity cores.

5. MICROBURST CHARACTERISTICS

Six independent microbursts were observed from these storms. The sixth microburst became part of a microburst line (Hjelmfelt and Roberts, 1985) which lasted for two hours. These microbursts are described in Table 1. A few other small-scale divergence features were observed which did not reach microburst intensity.

The microbursts described here were all of less than the average strength of 24 m s^{-1} radial velocity differential, ΔV, obtained for the entire JAWS data set (Wilson et al., 1984). Microburst 6 was the strongest, reaching 22 m s^{-1} maximum velocity differential. The distance between maximum approaching and receding velocities, ΔD, ranged from 2.3–4.0 km, while the JAWS average was about 3.3 km. The average total diameter, D_t , of the outflows to the outer convergence maximum was about 5 km. Downdraft diameters (>5 m s^{-1}) at 1-1.5 km AGL ranged from 1.2-1.6 km. Outflow depths were about average for JAWS microbursts, ranging from 0.6–1.4 km.

8

Table 1. MICROBURST OUTFLOW CHARACTERISTICS*

Microburst	Time of max (MDT)	ΔT (min)	Total lifetime (min)	Location from CP-2 (AZ/range)	ΔV at max (ms^{-1})	ΔD at max (km)	Total diameter D_ℓ (km)	Downdraft diameter $>5m\,s^{-1}$ (km)	Depth of outflow (km)	Morph. type	Decay mode	PAM Detection
1	1550	16	27	135/20	18	3	5.0	—	0.6	Isolated	Weakened	Yes
2	1609	4	9	125/27	14	2.5	4.8	—	0.8	Embedded	Weakened	No
3	1614	10	15	135/25	18	2.5	6.0	1.2	1.1	Embedded	Became Lg. Scale	Q
4	1615	6	11	122/32	12	2.0	3.2	1.6	1.4	Embedded	Became Lg. Scale	—
5	1623	9	15	140/20	16	2.3	5.0	1.4	0.6	Isolated	Weakened	Yes'
6	1624	10	20	162/23	22	4	4.8	1.4	0.9	Embedded	Became part of line	Yes'
Line**	1639	24	120	—	27	3	6	—	1.0	Line	Weakened	Yes'

* See text: Section 5

Q Questionable

' Also detected by single station methods

** No. of simultaneous microbursts along line—max $\geq$ 6, aver $\geq$ 3

Lifetimes* for the microbursts were slightly longer than average. Growth times from initial surface divergence to maximum strength, ΔT, were a little longer than the JAWS average of 6.4 min, ranging from 4 min to 16 min with an average of almost 9 min. The total lifetimes of these microbursts, until the outflow decayed below microburst intensity by dissipation or grew to larger scale, averaged about 17 min. During their lifetimes, little movement was observed; none of the microbursts moved more than 3 km.

The microburst line achieved a maximum of 27 m s^{-1} differential velocity and lasted for about two hours. It had an average length of 21 km and an average total width of more than 6 km. At one time there were at least six microbursts occurring along its length and, on the average, three component microbursts could be identified at any one time. All together, more than 20 separate microbursts were produced during the lifetime of the line. This number rises above 40 if reintensifications (or new pulses) of microbursts, after falling below microburst intensity for several minutes, are included.

The PAM network detected Microbursts 1, 5, and 6 and the microburst line well, showing strong divergence features in the network wind field (Wilson and Carpenter, 1983). Microbursts 5, 6, and the line were also detected by single station methods (Fujita, 1985; Bedard and LeFebvre, 1986). Microburst 3 was observed by PAM (see Fig. 5 below), but detection without *a priori* knowledge would have been unlikely. Microburst 2 occurred near the edge of the network and was not detected, and Microburst 4 occurred outside the network.

The storms which produced these microbursts were vigorous thunderstorms with peak observed reflectivities exceeding 65 dBZ aloft. At maximum intensity all of the microbursts occurred within reflectivity cores which exceeded 45 dBZ at 500 m AGL. Maximum radial shear values observed by single Doppler radar exceeded 6 x 10^{-3} s^{-1} in all cases.

6.   MULTIPLE DOPPLER RADAR ANALYSIS

In this section the structure and life cycle of some of the microbursts are examined in more detail. In order to study the structure of the shallow microburst outflow, scanning strategy in JAWS concentrated on high-resolution, low-elevation scans using a very small radar network. This strategy is incompatible with obtaining data to cloud top in useful time periods. In this case, only single Doppler data from CP-2, which did scan to cloud top, is available above cloud base.

Figures 5 and 6 depict the lowest-level horizontal winds derived from radial wind data from all three project Doppler radars. The analyses are presented on a 54 x 54 horizontal grid with grid intervals of 0.3 km in the horizontal and 0.4 km in the vertical. The radars are located as follows: CP-2 at (0.0,0.0); CP-3 at (14.2,-11.2); and CP-4 at (10.4,-25.4). Reflectivity contours are at 10 dBZ intervals beginning at 30 dBZ. Figure 5, analyzed for 1612, shows the flow pattern near the time of maximum intensity of Microburst 3 and just before Microbursts 5 and 6 become visible at the surface (see locations 3, 5,

---

* The accuracy of time estimates for JAWS microbursts is limited by the 2-2.5 min update rates for radar scanning.
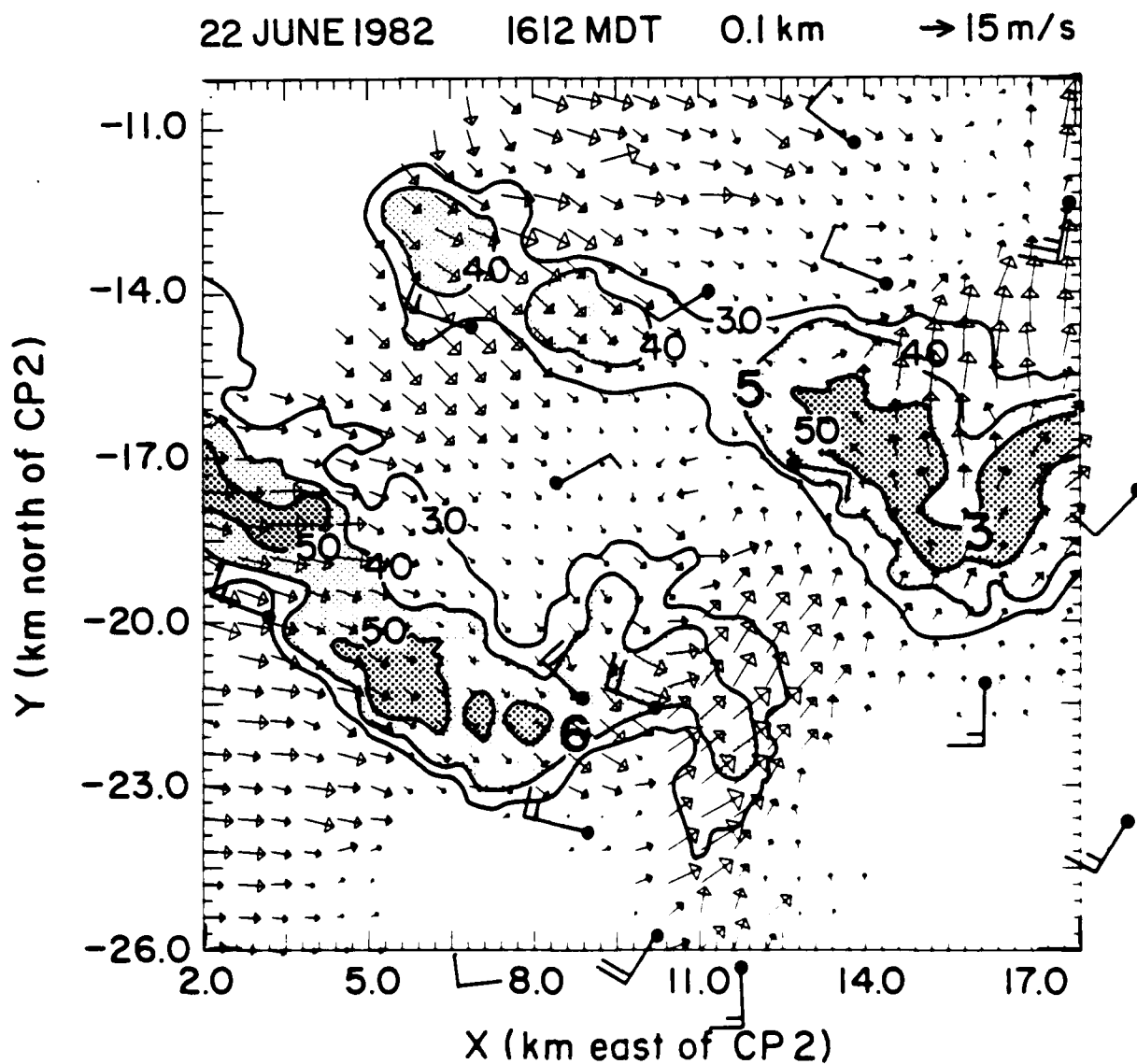
Figure 5. Horizontal winds and reflectivity contours for the lowest level from multiple Doppler analysis for 1612 MDT. Reflectivities are contoured in 10 dBZ increments beginning at 30 dBZ; light shading > 30 dBZ, heavy shading > 50 dBZ. Every other vector is plotted and wind arrows are scaled as shown at upper right. Microbursts studied include those that form at locations 3, 5, and 6. The PAM winds are plotted with one full barb for each 5 m s^{-1}.
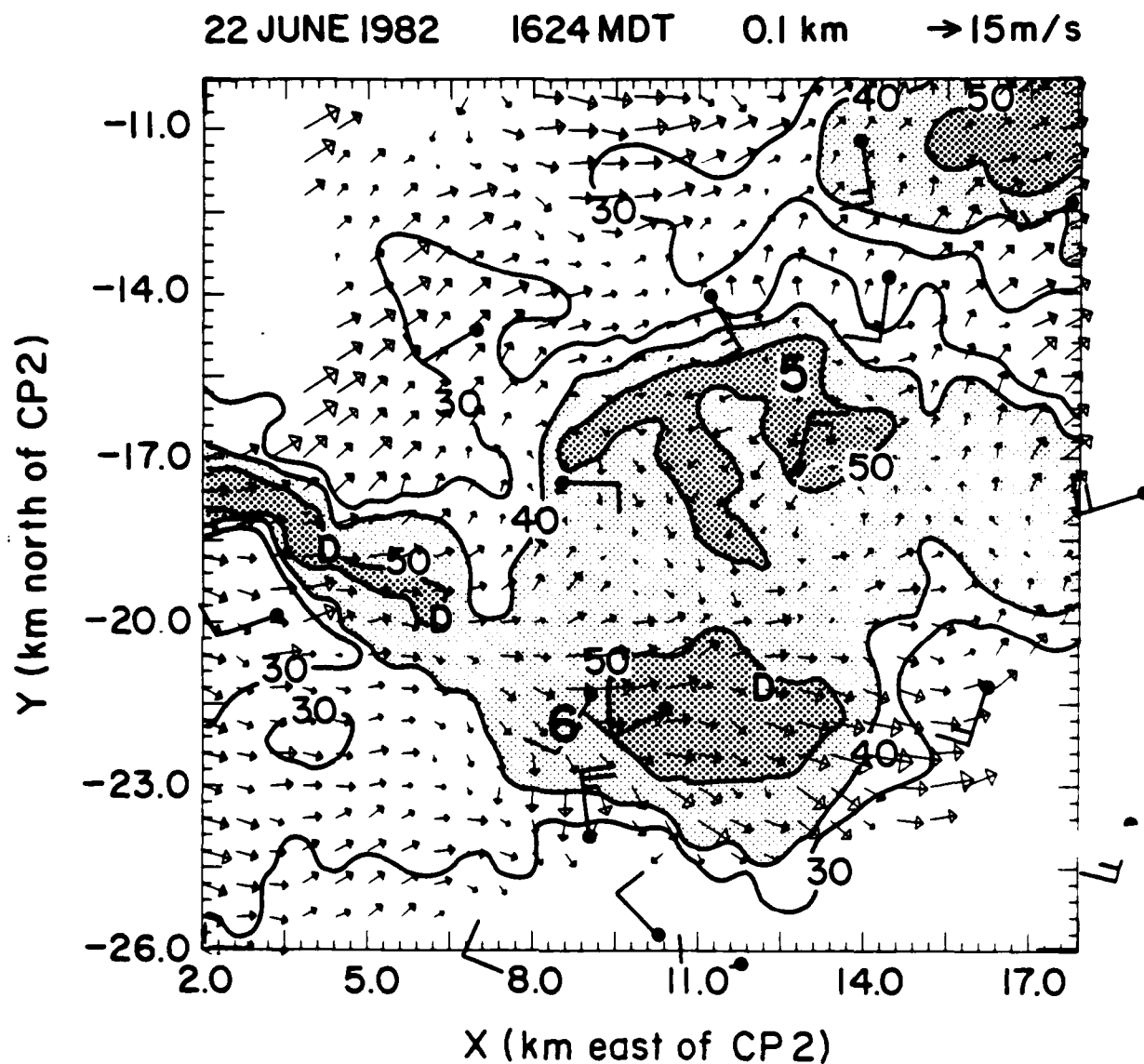
11

Figure 6. Horizontal winds and reflectivity contours for lowest level analysis at 1624, as in Fig. 5. Note microbursts at 5 and 6. Divergence centers along developing microburst line are indicated by D. The PAM winds are plotted with one full barb for each 5 m s^{-1}.

and 6 in the figures). Microburst 4 is off the figure to the east at (26,-17). Figure 6, valid at 1624, shows Microbursts 5 and 6 near their peak intensity.

In general, comparison of the flow patterns reveals increasing development of the storms and flow around and diverging out of reflectivity cores. The reflectivity patterns indicate development during this time period to the west and north in the northern storm and to the east in the southern storm. Considerable merging and expansion are apparent at 1624 as compared to 1612. These features and developments are seen up to mid levels (> 5 km). Movement of the storms is small and is masked by development. These very low-level plots show grid-averaged reflectivities exceeding 50 dBZ, but data from CP-2 reveal that the storm contained reflectivities > 65 dBZ aloft with small areas of > 60 dBZ found within precipitation cores to the surface.

At 1612, the environmental flow in the western and northwestern part of the analysis is dominated by flow from the west to northwest, while in the southeastern part of the grid, southerly flow dominates (see Fig. 5). Generally weak velocities are found in the convergence zone extending south-southwest to north-northeast across the grid. This flow is in agreement with the surface network data shown earlier in Fig. 4.

Microburst 3 is seen as a strong area of divergence associated with the 50 dBZ core of the northern storm at (16.1,-17.6). Microburst 3 is embedded in strong southerly flow and exhibits a strongly asymmetric form (see Fig. 9 below). The divergence of the southerly flow caused by Microburst 3 is also observed in the PAM surface winds. At the location where Microburst 5 will occur, weak flow with convergence is seen and reflectivity values are < 45 dBZ.

An intense cyclonic circulation along the convergence line is centered about a reflectivity appendage at the northern edge of the southern storm (11.0,-17.9). This circulation shows good vertical continuity to heights above cloud base. A small-scale updraft-downdraft couplet is associated with this circulation, similar to that discussed in Wilson (1986). No funnels or tornadoes were reported, but all JAWS observers were screened by intervening storms. The PAM network, however, recorded a strong mesoscale circulation centered at this location at this time. Vorticity calculated from Doppler observations reached $3 \times 10^{-2} s^{-1}$. We speculate that the strong shear along the boundary-layer convergence line caused by the collisions with the gust front and the northwesterly surge may have been responsible for this circulation. This circulation does not appear to have an intimate physical connection to the development of the microbursts and will not be considered in detail here.

Low-level divergence from the southern storm is not of microburst character and only small areas of > 50 dBZ appear near the surface at this time. There is little to indicate the imminent appearance of Microburst 6 at (8.0,-21.0).

At 1624 a 50 dBZ contour is centered directly over Microburst 5 and a symmetric divergent flow pattern is apparent. The microburst winds impinge upon countering flows in some directions, creating strong convergence, causing the flow to turn, and limiting the maximum velocities achieved by the microburst winds. The divergence to the southeast of Microburst 5 is the remnant of Microburst 3 which has become less intense and larger in scale.

The two storms now have merged precipitation shafts with 30 and 40 dBZ echo bridging between them. The small-scale circulation pattern which had existed in the space between the storms has now largely dissipated. Most dramatic, however, is the disappearance of the convergence line. The most striking feature of the overall flow pattern just 12 min earlier is being destroyed by the strong microburst outflows.

The southern storm shows strong divergence from Microburst 6 emanating from the vicinity of a 50 dBZ core. Microburst 6 developed in strong westerly flow. Therefore, the flow pattern is strongly asymmetric, similar to Microburst 3. Figure 6 also shows the developing microburst line with generally divergent flow extending across the southern part of the region. The beginnings of several discrete divergence centers, D, can be seen as a part of the developing line. Microburst 6 developed within a 55 dBZ core (see Fig. 16 below). As the microburst neared maximum intensity, surface reflectivity began to weaken at the center of the microburst and new high-reflectivity cores began to appear nearby. This may be related to microburst line development, but a similar occurrence has been observed in an isolated low-reflectivity microburst by Kropfli (1986).

The PAM network indicates flow patterns in substantial agreement with the above radar analyses. The outflows from Microbursts 5 and 6 were observed by the PAM surface stations (see Fig. 6). This is reassuring given the considerable ground clutter contamination which must be treated in the radar analysis. Figure 7 shows gridded PAM winds (Wilson and Carpenter, 1983) for 1624 over the same area as displayed for the radar analysis in Figure 6. The curved flow around the storms and the divergence from Microbursts 5 and 6 are prominent features of the surface wind analysis as well as in the radar data.
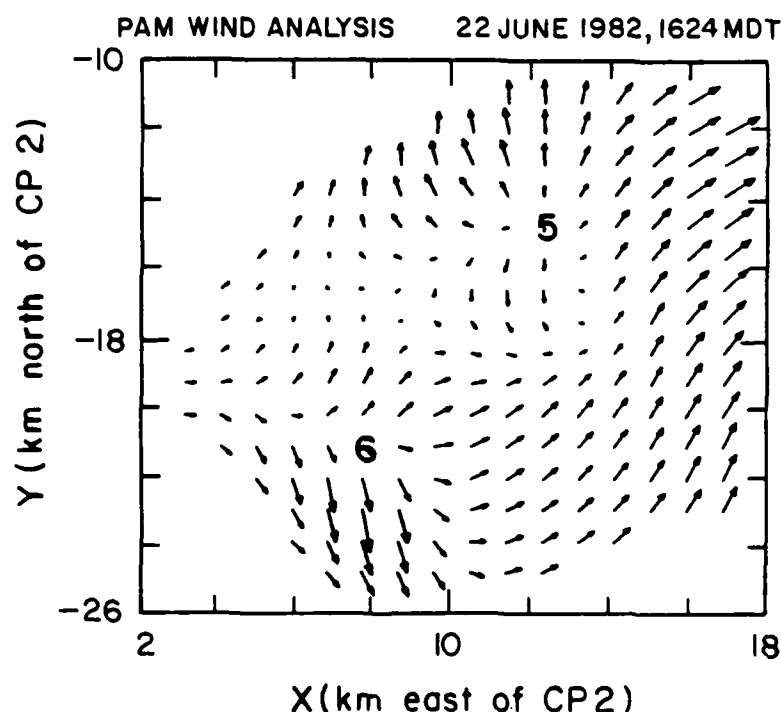

Figure 7. Gridded 1-min average wind vectors from PAM surface observations. Vectors are drawn to scale of 14 m s^{-1} to one 2 km grid interval.

14

Figure 8 shows the three-dimensional reflectivity structure of the storms at 1612. The two dark 45 dBZ cores on the left correspond to the two precipitation regions shown in Figure 5. The core to the right is producing Microburst 4 and the core in the back of Figure 8 is to the north of the area displayed in Figure 5. These cores are embedded in a large cloud line enclosing them all. Each core corresponds to a tower embedded in the 20 dBZ echo (halftone) extending to, or above, the 9-km level.

6.1 *Microburst 3*

Figure 9 shows the low-level flow for Microburst 3. The absolute winds are shown in Figs. 9a and 9b, for 1612 and 1617 respectively, and reveal a very asymmetric pattern dominated by a strong southerly component. At 1617, just after maximum intensity, the low-level flow field exhibits somewhat stronger divergence than earlier. In Fig. 9c, the mean wind of 6.7 m s^{-1} from 168° Az is removed from the 1617 field. (This mean wind is in agreement with the larger-scale environmental low-level flow over this area, as shown in Fig. 4.) The microburst divergence is more clearly seen in Fig. 9c. Divergence exceeds 10^{-2}s^{-1}.

At 1612, rotation in the area of downdraft is seen at 1.3 km altitude (Fig. 10a). The rotation occurs within the area of downward motion; while not centered over the downdraft maximum, it is not on the updraft-downdraft gradient. The rotation decreases above this height. By 1617, the rotation has disappeared and convergence is seen above 1 km (Fig. 10b). Estimated peak downdraft velocities at this height exceed 10 m s^{-1}. Figure 6, shown earlier, indicates that by 1624 this microburst has become a less intense, larger-scale outflow.

6.2 *Microburst 4*

Microburst 4, not shown, is quite similar to Microburst 3 at low levels. Occurring in the same low-level southerly flow, Microburst 4 exhibits a similar embedded outflow structure. Aloft, convergence is seen at 1612 below cloud base from 2-2.8 km AGL. Doppler data suggest some cyclonic vorticity is present at 1617 above 2.5 km located in the vicinity of the microburst downdraft.

6.3 *Microburst 5*

Figure 11 shows the surface-level evolution of Microburst 5. At 1612 (Fig. 11a), the flow is dominated by convergence and deformation along the large-scale convergence boundary discussed in Section 3. Five minutes later, at 1617 (Fig. 11b), a small divergence center is seen, centered near (12.8,-15.5). Microburst 5 is at maximum intensity at 1624 (Fig. 11c). A symmetric outflow with divergence $>10^{-2}$s^{-1} is shown. This microburst weakens and disappears by 1632.

The quick change from convergence and generally upward motion to mature microburst is quite striking. It implies that the parent storm represents more of a classical Byers and Braham (1949) thunderstorm life cycle as opposed to the long-lived supercell which is usually associated with violent weather.
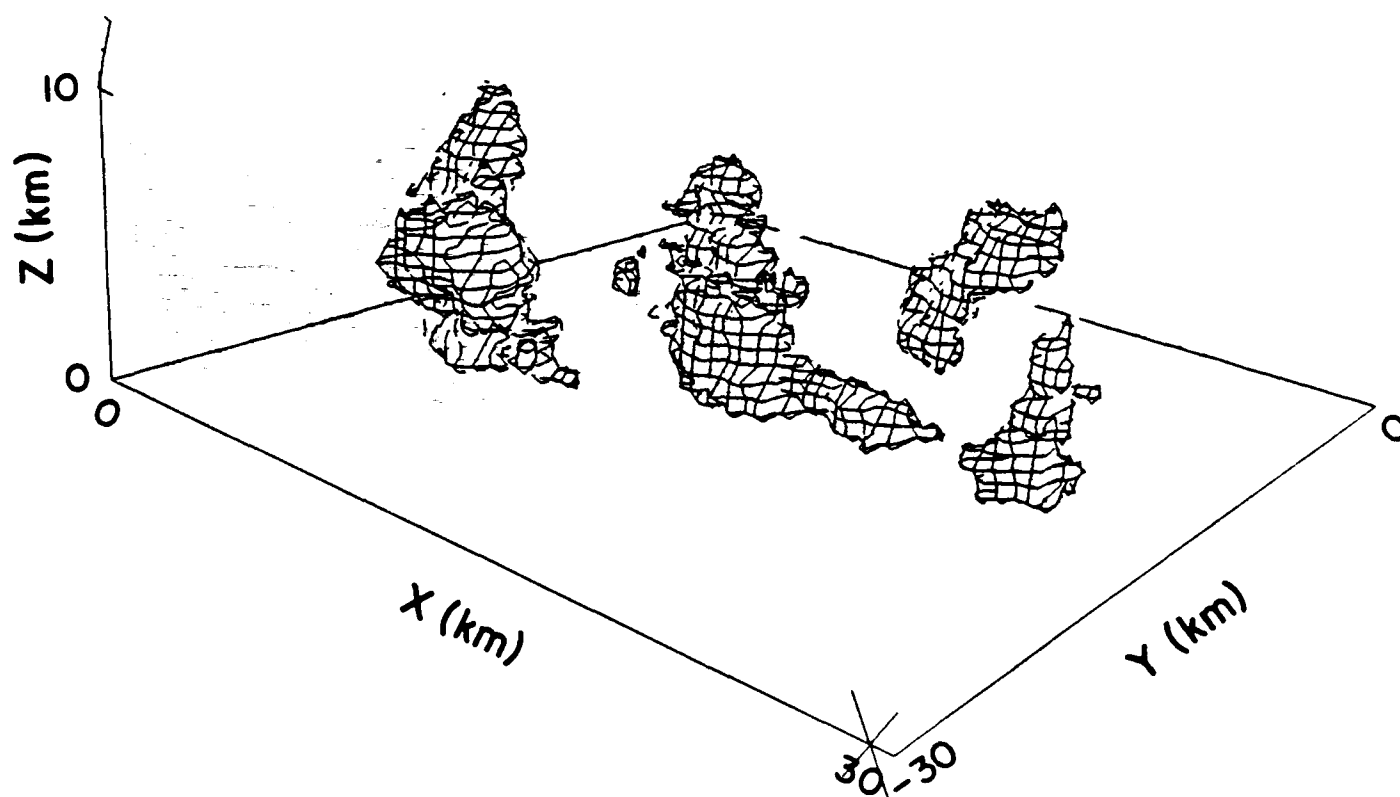
Figure 8. Three-dimensional reflectivity structure of storm at 1612 MDT. Dark reflectivity cores are $\geq$ 45 dBZ. Halftone shows reflectivity $\geq$ 20 dBZ. The O° km AGL level not shown. Two cores at left correspond to those shown in Fig. 5.

16
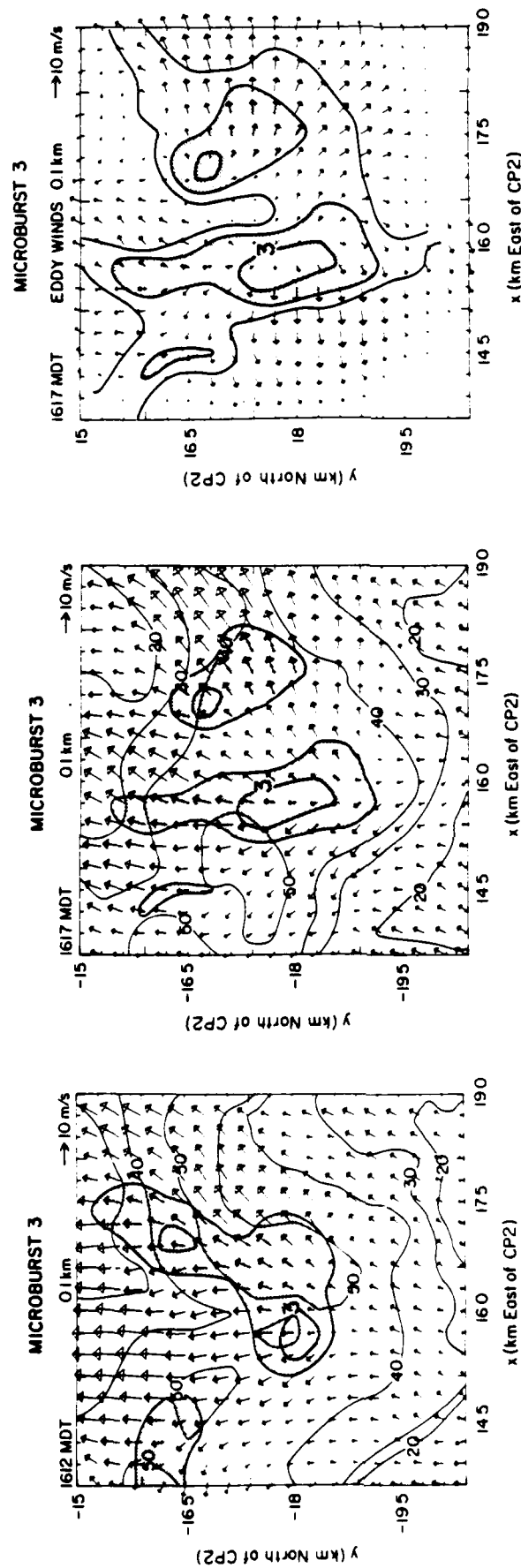
Figure 9. Horizontal winds and reflectivity contours at lowest level of analysis for Microburst 3. Wind arrows are scaled as shown in upper right. Divergence is contoured in $5 \times 10^{-3} s^{-1}$ increments starting at $5 \times 10^{-3} s^{-1}$ and shaded. Reflectivity contours are given in 10 dBZ increments starting at 20 dBZ. Center of microburst is indicated by number 3. (a) 1612 MDT, (b) 1617 MDT, (c) eddy winds (mean wind removed) for 1617 MDT; reflectivity not shown and $2 \times 10^{-3} s^{-1}$ divergence contour added.
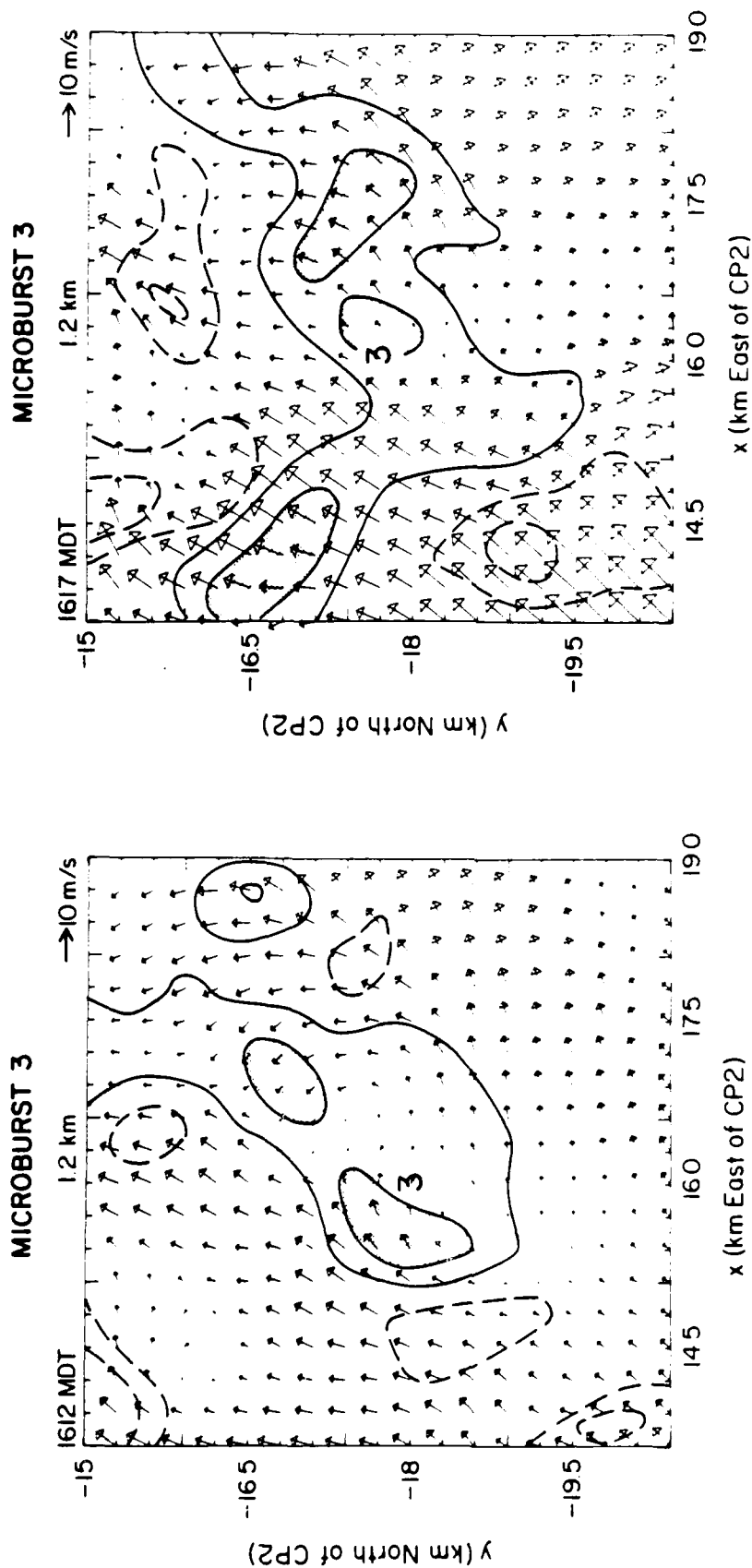
Figure 10. Horizontal winds and vertical velocities at 1.3-km level for Microburst 3. Vertical velocity contours are at 2, 6, 10 m s^{-1}. Downdrafts (solid contours) > -6 m s^{-1} are shaded and updrafts (dashed contours) > 6 m s^{-1} are hatched. Center of surface microburst is indicated by number 3. In (a), 1612 MDT, note rotation in area of downdraft, but in (b), 1617 MDT, there is none.

18
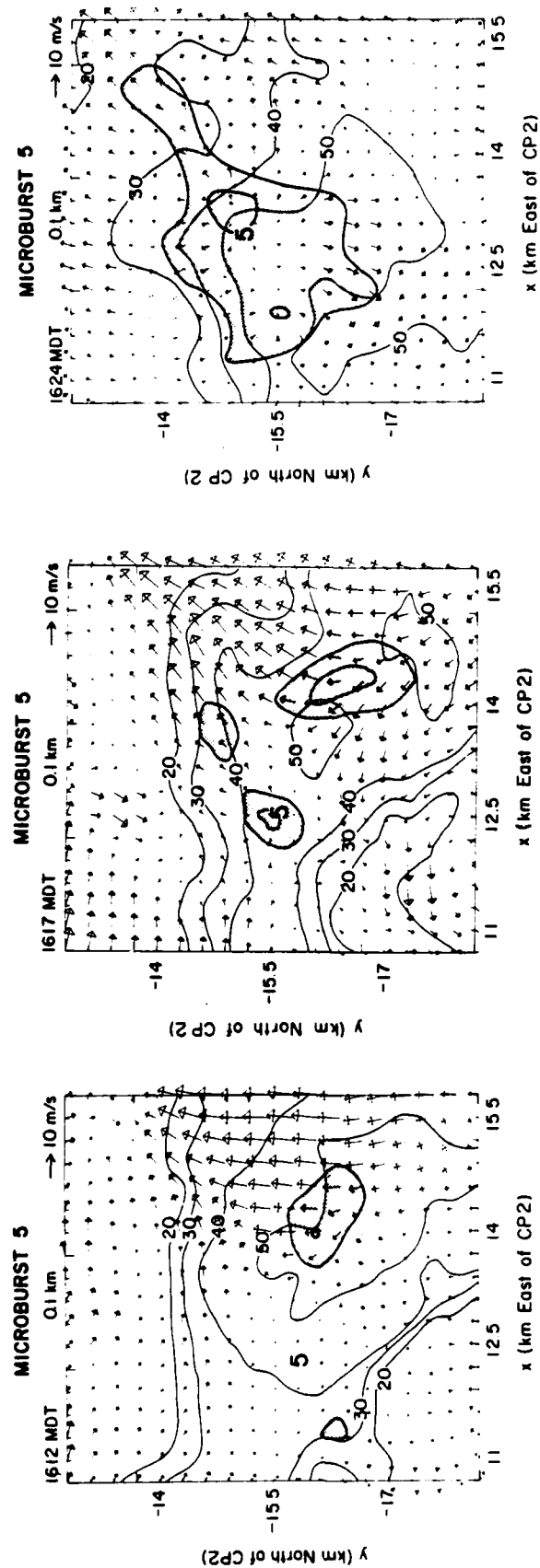
Figure 11. Horizontal winds and reflectivity contours at lowest level of analysis for Microburst 5, as in Fig. 9. Times of analysis are (a) 1612 MDT, (b) 1617 MDT, (c) 1624 MDT.

19

The low-level reflectivity near the microburst center increases with time and by 1624 it approaches 60 dBZ. The pattern aloft also indicates intensification and descent of precipitation.

The vertical outflow structure, not shown, reveals that this is a shallow microburst with most of the divergence confined below 0.5 km. Downdrafts in excess of 12 m s^{-1} are found at 1 km. Detailed reflectivity patterns from CP-2 indicate a low-reflectivity notch just below cloud base. Doppler velocities from CP-2 also indicate convergence between 2 km and 2.8 km. At 1624 a small-scale rotation is centered over the downdraft at about (12.8,-15.2) near 1 km altitude (see Fig. 12). Outflow at 1627, not shown, during decay of the microburst exhibits considerable cyclonic curvature. Unfortunately, multiple Doppler analysis does not extend above 1.3 km over this part of the network. Significant rotation does not appear in either the multiple Doppler analysis or single Doppler radial wind fields from CP-2 at earlier times.

The PAM network sampled this microburst thoroughly to show a well-defined divergence signature. Divergence greater than 4 x 10^{-3} was obtained from analysis of the surface network data for 1624 (average station spacing was about 3 km). Average temperature decreases of 2°C and dew point increases of 3°C were recorded as the microburst winds reached nearby stations. Relative humidities increased but remained below 70%. Pressure perturbations were less well defined. These observations suggest descent of cool, negatively buoyant air and considerable evaporation potential.

6.4 *Microburst 6*

Figures 6 and 7 show the low-level outflow as observed by Doppler radar and PAM for Microburst 6, which was produced by the southern storm. This microburst is embedded in west-northwesterly environmental flow. At 1624 the divergent flow is well defined. An elongation of the divergence is forming to the northwest and east as the microburst line develops through this area. Peak divergence for Microburst 6 exceeds 1.4 x 10^{-2}s^{-1} from the Doppler analysis at 1624. The surface network indicates divergence greater than 6 x 10^{-3}s^{-1} at this time. Surface network stations influenced by Microburst 6 experienced average temperature decreases of roughly 1.5°C and dew point increases of 2.5°C. Relative humidity increased but maximum values did not exceed 70%.

Aloft rotation (not shown) is found at 1612 over the location of Microburst 6 from about 1.5 km to near cloud base at 2.8 km (the highest level for which multiple Doppler data are available). This rotation appears to be located approximately on the updraft-downdraft gradient. By 1617, however, only general convergent flow is seen at these levels. Peak downdraft velocities approached 10 m s^{-1} at 1.7 km AGL. The outflow from this microburst is deeper than that of Microburst 5, with some divergence present at 1 km altitude.

6.5 *Microburst Line*

Microburst 6 is part of a developing larger-scale microburst line, which by 1641 extends south-southwest to east-northeast across the network. Figure 13 shows PAM winds and the divergence line axis (heavy dark line) based on a composite of single Doppler

20
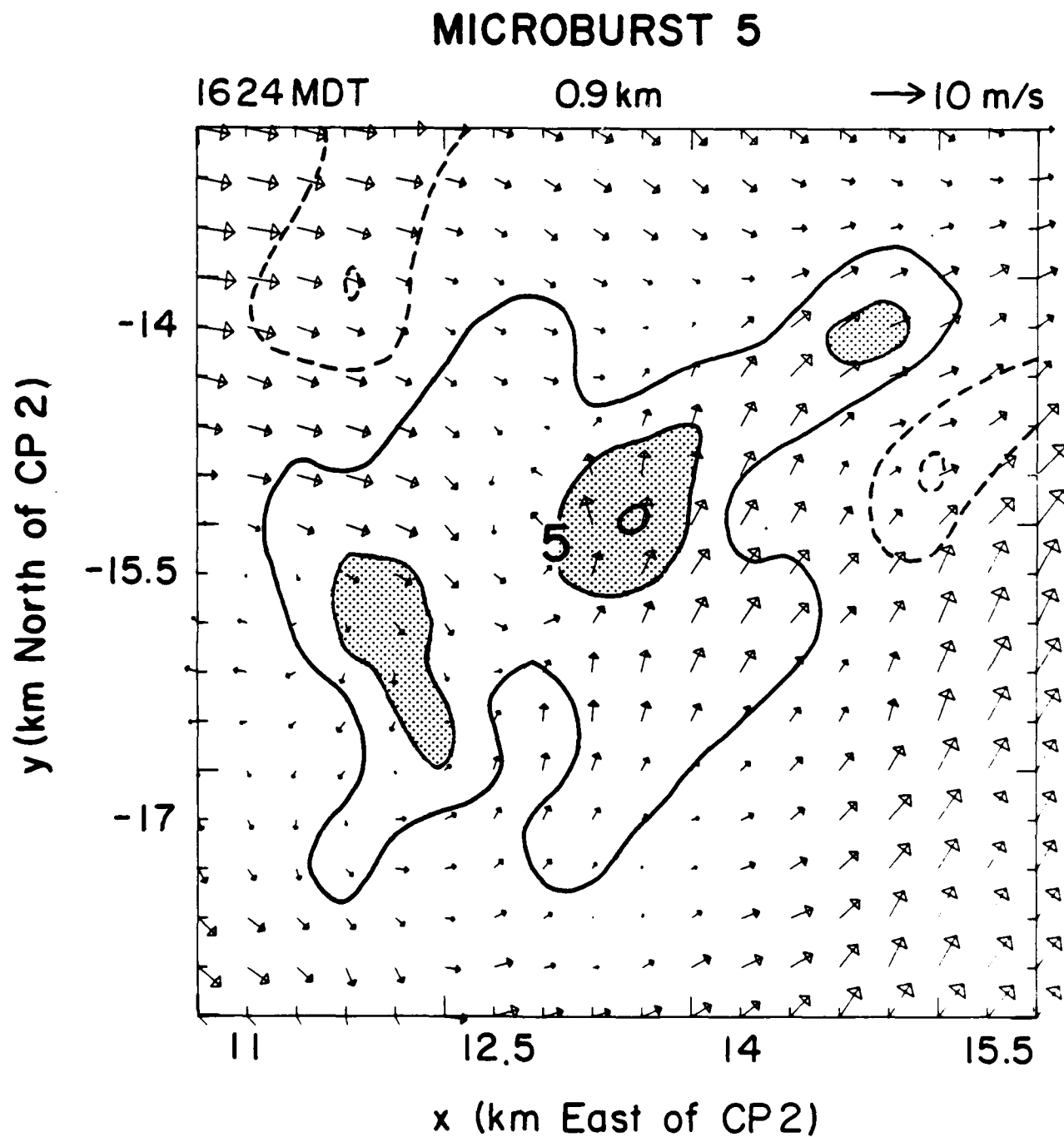
Figure 12. Horizontal winds and vertical velocities at 0.9 km for Microburst 5 at 1624 MDT, as in Fig. 10.

PAM WINDS

22 JUNE 1982   1639 MDT
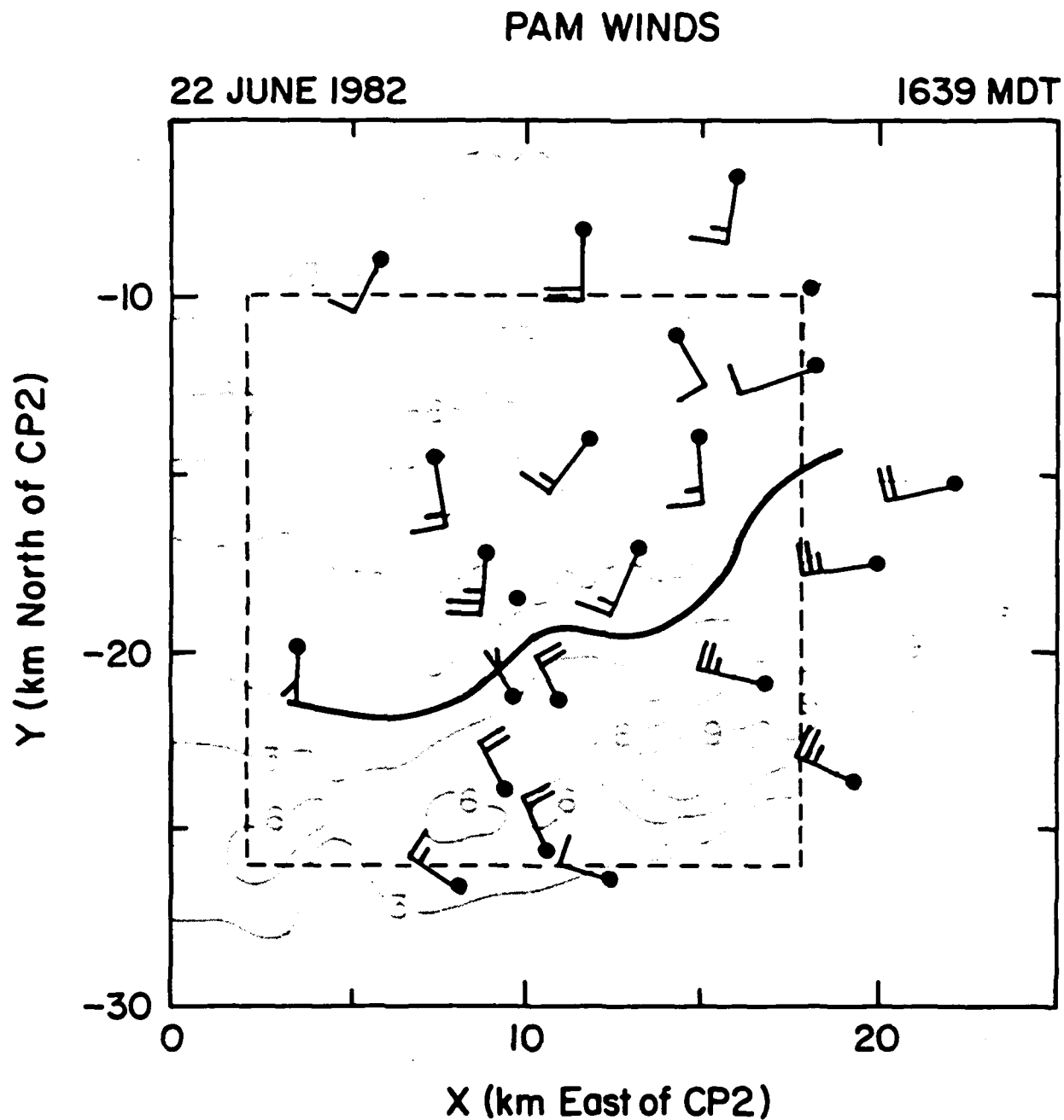
Figure 13. Map of surface winds observed by the PAM network at 1639 MDT. One full wind barb equals 5 m s^{-1}. Divergence line as observed by Doppler radar is shown by heavy black line. Thin dotted line denotes boundary of radar analysis in Fig. 14. Smoothed radial velocities observed by CP-2 radar shown in halftone negative values indicate component toward radar; positive values indicate flow away from radar.

winds. The divergence line extends across the network for almost 2C km. The PAM winds show strongly divergent flow all along the line. Smoothed single Doppler radial velocities from CP-2 (halftone) also show the linear divergence pattern.

A more detailed view from low-level multiple Doppler analysis is shown in Figure 14. The more or less continuous line of divergence on the large scale is made up of a number of outflows emanating from individual centers, D, and represents the superposition of these individual outflows. Comparison of Fig. 14 with Fig. 5 shows that the entire character of the low-level flow field has changed. The earlier flow toward the convergence line has now reversed to divergent flow outward from the microburst line.

Figure 15 shows the three-dimensional reflectivity structure of the storm at 1641. Comparison to the structure at 1612, Fig. 8, reveals that the area of 45 dBZ echo which had been in deep cores extending above 9 km AGL at 1612, extends only to about 4 km at 1641. The cloud boundary, as estimated from the 20 dBZ surface, is much larger at 1641 than at 1612. The decay of the deep 45 dBZ cores suggests a decay of updraft strength.

This line existed for over two hours. Different points strengthened and weakened at different times. At any one time the maximum differential in the Doppler radial velocities, ΔV, observed along the line was usually in excess of 18 m s^{-1} (with a peak value of 27 m s^{-1} at 1640), while the average ΔV exceeded 12 m s^{-1}. The mean distance between radial velocity maxima was 3 km, while the total width from outer-edge to outer-edge was estimated to be in excess of 10 km. The outflow depth was similar to that of the individual microbursts discussed earlier, averaging about 1.0 km. Eventually, after 1800, the line decreased below microburst intensity and dissipated.

6.6 *Radar Analysis Summary*

Based on single and multiple Doppler analyses, the microburst outflow features observed on this day may be classified into three groups: isolated, more or less symmetric outflows (Microburst 5); outflows embedded in strong low-level flow which reveal their diverging outflow structure most clearly only when the mean environmental flow is removed (Microbursts 3, 4, and 6); and the microburst line. Microbursts 1, 2, and 5 decayed by weakening; Microbursts 3 and 4 grew into less intense, larger-scale outflows. Microburst 6 became part of the microburst line. Aloft, several features were identified which may relate to microburst formation mechanisms. These are considered in more detail in the next section.

7. MECHANISMS OF MICROBURST FORMATION

A number of mechanisms have been proposed that may cause or contribute to downdrafts of microburst intensity. Negative buoyancy production due to evaporation of falling rain (Brown et al., 1982; Kamburova and Ludlam, 1966) and melting of ice particles is an especially attractive explanation for microbursts from high-based cumulus clouds in a dry environment (Knupp, 1985). Shedding from melting hail could produce a continuing supply of small drops (Rasmussen et al., 1984), important for evaporational cooling (Kamburova and Ludlum, 1966). An unstable subcloud layer permits greater penetration of the downdraft below cloud base by reducing the rate at which compressional heating causes
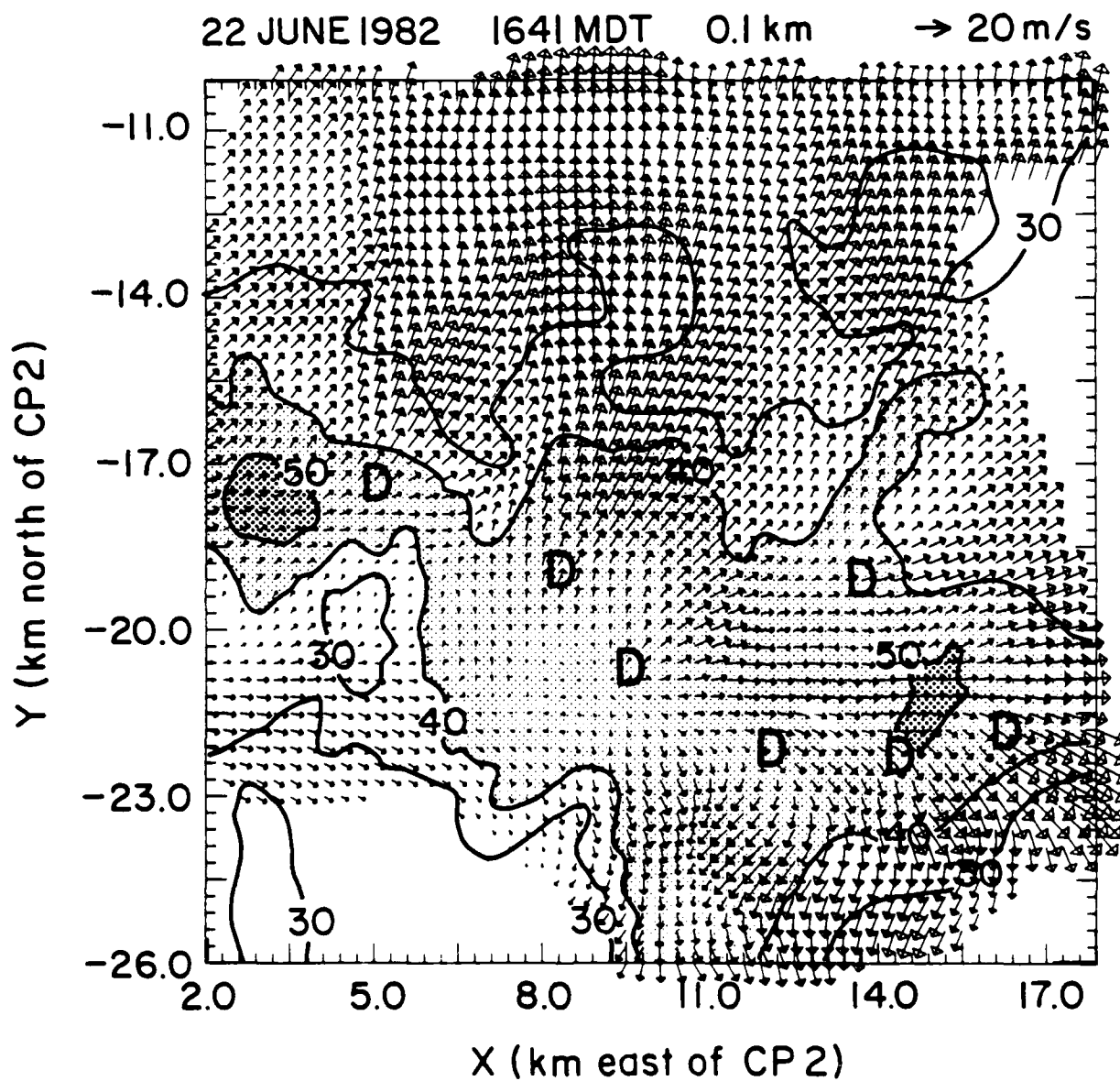
22 JUNE 1982   1641 MDT   0.1 km   → 20 m/s

Figure 14. Horizontal winds and reflectivity at 1641 MDT, as in Fig. 6, except every vector is plotted. Divergence centers are denoted by D.
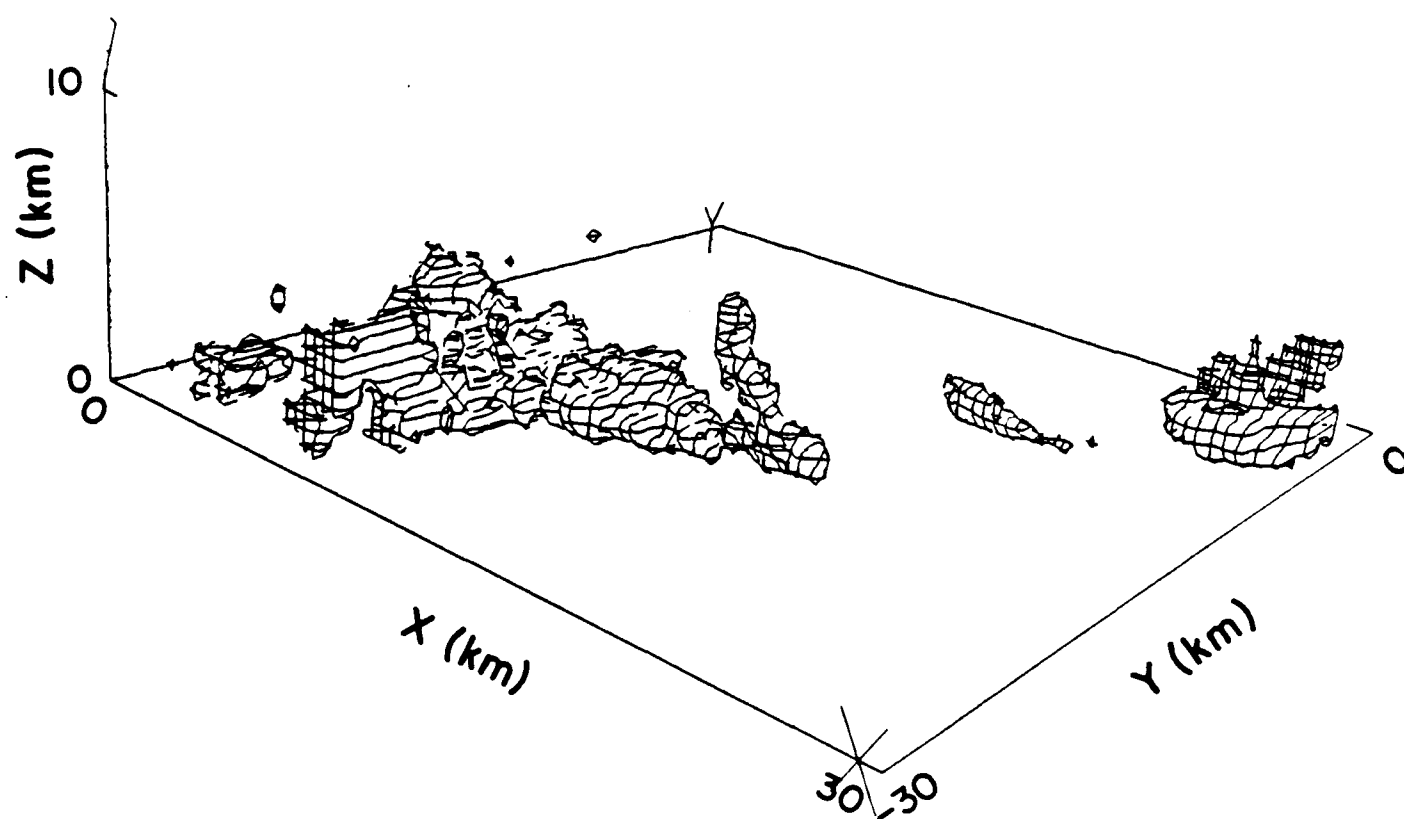
24

Figure 15. Three-dimensional reflectivity structure of storm at 1641, as in Fig. 8.

the virtual temperature of the descending parcel to approach that of the environment (Srivastava, 1985). Calculations of the effects of frictional drag from falling precipitation (Clark and List, 1971; Kamburova and Ludlam, 1966) indicate that precipitation loading can potentially produce strong downdrafts in heavy rain.

Rotation of the downdraft may indicate dynamic factors or may be merely a result of conservation of angular momentum and the acceleration of the descending air in the downdraft. Fujita and Wakimoto (1983) hypothesized that rotation, which is frequently observed in connection with microburst downdrafts, acts to collect hydrometeors and concentrate the downdraft. Modeling results of Klemp and Rotunno (1983) suggest that vertical pressure gradients dynamically induced by tornado parent circulations may produce strong downdrafts. Similar dynamically-produced pressure gradients were observed in the severe cold frontal rainband studied by Carbone (1983). The source of the pressure gradient in this last study was rotation related to instabilities along a very strong frontal shear line. For pressure gradient forcing, the rotation is situated dynamically on the updraft-downdraft gradient. Dynamic forcing from rotation is most attractive as an important factor for microbursts from rotating supercell storms.

Several observations were made in the present study which are relevant to the above mechanisms. Table 2 identifies these features for each microburst. Five of the microbursts showed indications of rotation in or near the downdraft. In two cases the rotation was centered over the microburst downdraft, in one case rotation was observed on the updraft-downdraft gradient, and one case showed no indications of rotation. Timing and vertical continuity of the rotation was variable. Comparing Tables 1 and 2 we can see that in cases 3 and 6 the rotation occurred during microburst growth, while in cases 4 and 5 the rotation was not apparent before the time of maximum surface intensity. In Microbursts 3 and 5 the rotation appeared to be restricted to low altitudes, while in Microburst 4 rotation was at a maximum above cloud base.

Microbursts 1, 5, and 6 occurred along a strong boundary-layer convergence line; Microbursts 2, 3, and 4 occurred some distance away (see Fig. 4).

Descending reflectivity cores are indicative of descent or intensification of precipitation shafts. High reflectivities further indicate the presence of significant water loading. Each of the microbursts listed in Table 2 was associated with the descent of an identifiable reflectivity core or appendage of 50 dBZ or more. The cores were observed to descend from scan to scan, with intensification beginning at the surface roughly coincident with first low-elevation detection of the outflows. Peak surface reflectivities were attained just prior to maximum microburst divergence value.

The evolution of the vertical reflectivity structure for Microburst 6 is given as an example in Fig. 16, which shows a plot of the area of > 55 dBZ reflectivity over the location of the microburst as a function of altitude and time. The dotted line indicates the time of greatest area at each height. This line slopes downward with increasing time, suggesting a descending core (intensification of the precipitation shaft). This association appears to be common for microbursts in general (Roberts and Wilson, 1984). The intensified core begins to descend before divergence is first identified at the surface, shown by I, and reaches a maximum at the ground shortly before maximum microburst divergence is attained, at II. The closeness of the lines of constant area between 2 and 2.5 km just below the 0°C

Table 2. MICROBURST FORCING OBSERVATIONS

| Microburst	Rotation					Reflectivity			Convergence	
	Evidence	Time observed (MDT)	Location w.r.t. downdraft	Sense	Height (km AGL)	Descending core	dBZ (500m AGL)	Reflectivity notch ht. (km AGL)	Ht. of max (km AGL)	On/Near shear line
1	single Doppler questionable	1550	?	anti-cyclonic shear	1-1.3	yes	50	no	---	yes
2	single Doppler	---	---	---	---	yes	50	2-2.5	2.2	no
3	single & multiple	1612	over downdraft	cyclonic	1-3	yes	55	no	4.0	no
4	single	1615	?	cyclonic	3-3.7	yes	50	no	2.8	no
5	multiple	1624	over downdraft	cyclonic	.9-1.3	yes	60	no	1.3	yes
6	multiple	1612	updraft/ downdraft gradient	cyclonic	1-2.3	yes	60	1.7-2.5	2.3	yes
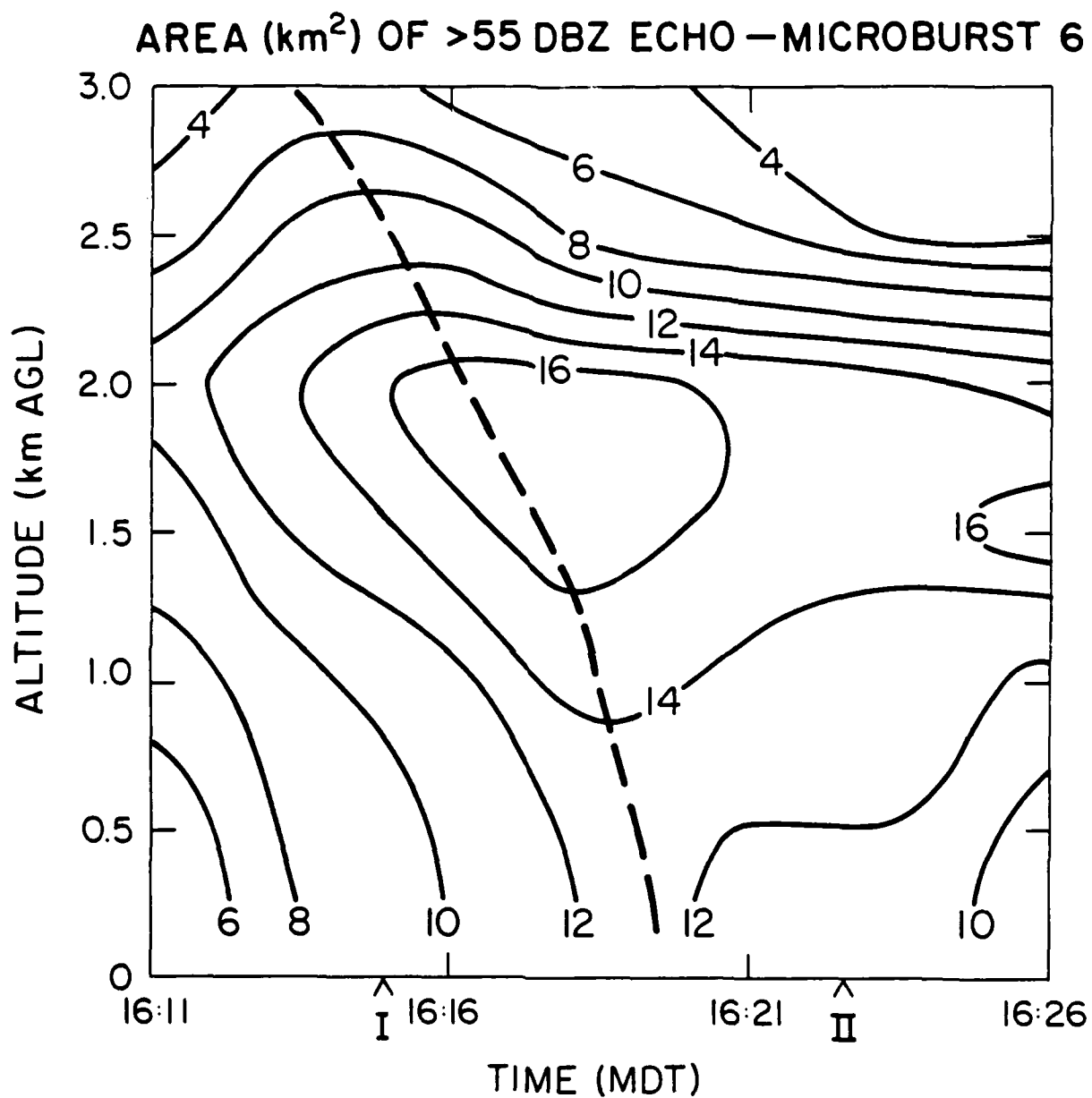
Figure 16. Area enclosed by 55 dBZ echo contour surrounding the location of Microburst 6 plotted as a function of altitude and time. Heavy dotted line indicates approximate time of maximum area at each height. Contours are for area in kilometers. I indicates time of first radar observation of surface divergence; II indicates time of maximum divergence.

temperature level represents a form of radar bright band. The maximum area achieved (17 km²) is also found just a little below the 0° C level, suggesting melting and water coating of graupel and hail. The area of > 55 dBZ echo decreases below this level.

Convergence aloft indicates potential source levels for downdraft air. Such convergence may indicate entrainment of dry air from the environment and production of negative buoyancy, or may represent mass adjustment in response to an accelerating downdraft at and below that level. A notch of lower reflectivity pointing toward the downdraft location, in conjunction with evidence of convergence, further suggests ingestion of dry or precipitation-free air. All of the microbursts except, perhaps, Microburst 1 showed indications of convergence in the upper part of the boundary layer below cloud base during the growth phase of the microburst. Two microbursts had identifiable reflectivity notches corresponding to this convergence. Surface relative humidities at affected stations remained well below saturation throughout microburst intensification. These observations suggest that evaporation might be important.

Cold cloud temperatures, reflectivities indicative of the presence of large ice particles, and the vertical-time structure of the precipitation core (Fig. 16), showing indications of a radar bright band, are evidence of melting.

In order to examine the role of microphysical and thermodynamic interactions in downdraft development and intensification, the model of Srivastava (1985) was applied to this case. This simple one-dimensional, time-dependent model is described by equations for raindrop evaporation, raindrop concentration, water substance, thermodynamic energy, and vertical air velocity. At the top of the downdraft, the pressure, temperature, relative humidity, vertical air velocity, and raindrop size distribution are specified. The environment of the downdraft is assumed to be quiescent and steady, and is specified by the height distributions of temperature and water vapor. The bottom of the downdraft is considered open. Calculations are presented for downdrafts developing in the subcloud layer. Ice phase is not considered, including the potentially important effects of diabadic cooling due to melting and sublimation.

Calculations were carried out using cloud base conditions based upon a special sounding taken at Denver at 1400 (Fig. 17). Surface conditions and intervening lapse rates of environmental temperature and humidity were adjusted from the sounding values on the basis of PAM surface data taken in close proximity to microburst touchdown. All PAM sites achieved maximum surface temperatures of approximately 26° C at about 1530. Surface conditions for each microburst at time of first detection, based on an average of nearby PAM stations, are shown in Table 3.

Cloud base was taken to be 600 mb with a temperature of about -0.8° C, just saturated with a mixing ratio of 6 g kg^{-1}. A 26° C surface temperature yields a 9.6° C km^{-1} lapse rate of temperature and a constant 6.0 g kg^{-1} mixing ratio. For simulations with reduced surface temperatures and enhanced humidities, a linear lapse rate from the surface through an assumed depth of cooling was used (see Fig. 17). One simulation, F, was run assuming an internal boundary layer capped by an inversion. Entrainment calculations assume a simple inverse-radius dependent lateral entrainment (Srivastava, 1985) for a 1-km radius downdraft. (Most microburst downdrafts in JAWS appear to have radii of ~1 km.)
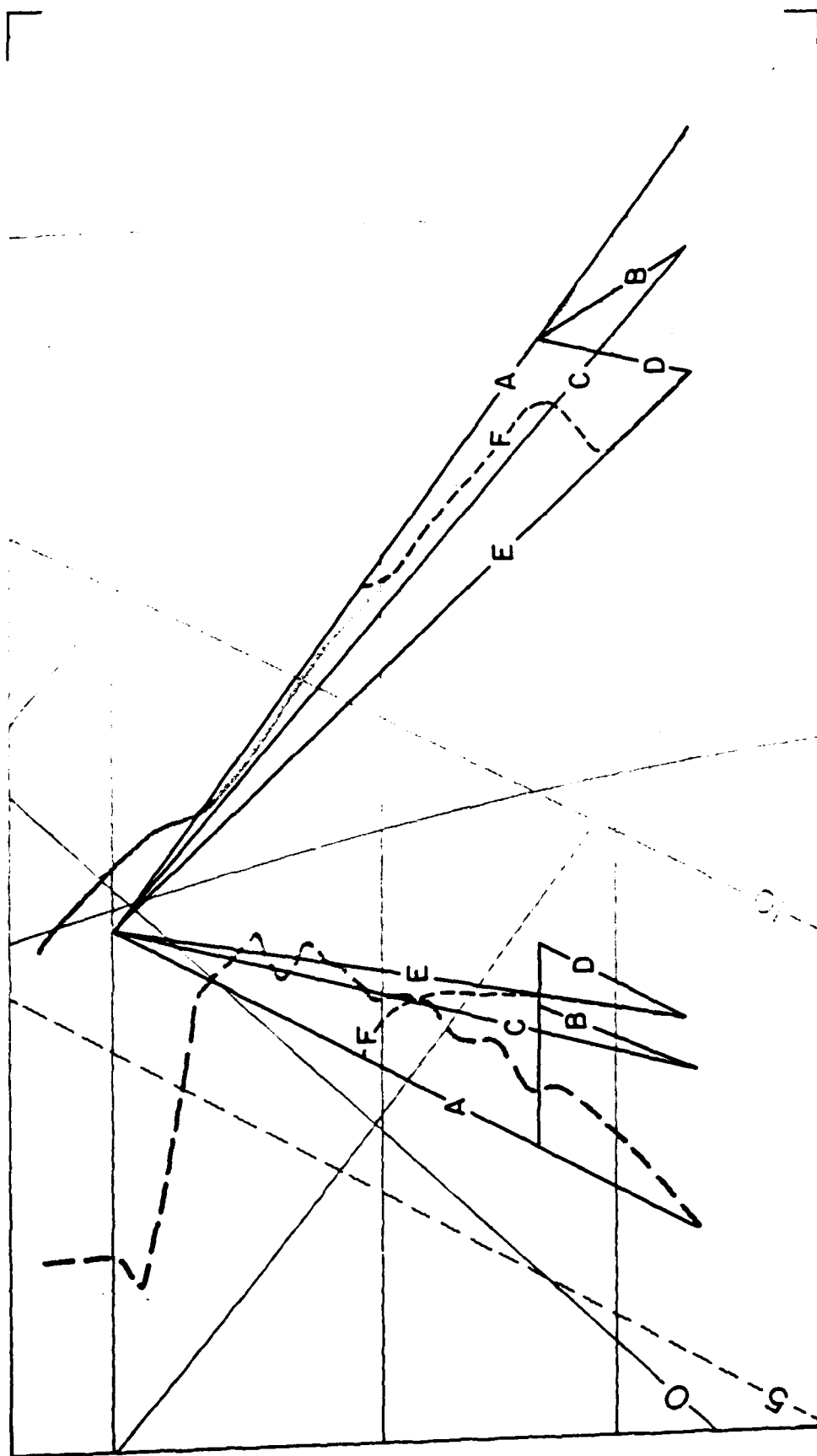
29

Figure 17. Lowest altitudes of Denver sounding for 1400 MDT, plotted on a Skew-T Log-P diagram, showing lapse rates used in the model calculations. Denver 1400 MDT sounding is given by a thick halftone line. Model soundings are labeled by letter (see Table 4).

Table 2 shows that all of the microbursts were associated with reflectivity cores > 50 dBZ.

Table 3. SURFACE CONDITIONS FOR MICROBURSTS

Microburst	Temperature* (°C)	Relative* humidity (%)	Mixing ratio (g kg^{-1})	Rainfall rate** max 1 min aver (mm hr^{-1})	Dist. to nearest station (km)
1	26	23	6.0	15	
2	21	42	8.2	60	1-2
3	23.5	34	7.5	45	2-3
4†	—	—	—	—	—
5	21.8	40	8.0	30	1-2
6	21.8	40	8.0	60	1-2

*Taken from average of nearest representative PAM stations at initial radar observation of outflow. Distance to station nearest microburst center is listed.
**Quantized in 15 mm/hr increments (0.25 mm).
†Microburst 4 occurred outside PAM network, conditions expected to be similar to Microburst 3.

The high reflectivities in this case indicate the probable presence of hail, suggesting that conservative estimates of precipitation rates should be used. Simulations were thus performed assuming an exponential initial drop size distribution given by Sekhon and Srivastava (1971) for 45 dBZ. This distribution is equivalent to a rainfall rate of 31 mm hr^{-1}. Actual maximum rainfall rates observed at microburst-affected PAM sites are shown for each microburst in Table 3.

Table 4 lists the simulations which were run and the resulting vertical velocity obtained at 2800 m below cloud base (equivalent to ground level). The model soundings are shown in Fig. 17. The runs for five degrees of cooling represent the extreme case. Only Microburst 2 encountered such strong deviations from the basic state. The results show that even with entrainment, vertical velocities in excess of 12 m s^{-1} are obtained for all cases except when cooling is assumed to extend through the entire boundary layer or an internal boundary layer has formed. JAWS analyses suggest that microburst downdrafts are typically in the neighborhood of 10-15 m s^{-1}. Multiple Doppler analyses suggest similar values for this day.

Simulations using different humidity lapse rates resulted in less than 0.5 m s^{-1} difference over a wide range of choices. An assumed initial drop-size distribution for 50 dBZ (74 mm hr^{-1}) produced a substantial increase in final vertical velocity, especially

31

Table 4. RESULTS OF DOWNDRAFT MODEL SIMULATIONS*

| Simulation | Surface conditions | | | | Simulated vertical velocity 2.8 km below cloud base (ms⁻¹) | | |
| | Temperature (0°C) | Relative humidity (%) | Mixing ratio (g kg^{-1}) | Depth of cooled layer (km) | 45 dBZ rain | | 50 dBZ rain |
					No Entrainment	Entrainment	Entrainment
A	26	23	6.0	---	20†	15	
B	23.5	34	7.5	0.8	19	13	18
C				2.8	15	11	
D	21	42	8.0	0.8	17	12	17
E				2.8	9	7	13
F**				1.2	14	9††	15

*See text and Fig. 17 for explanation
**F is with internal boundary layer (see Fig. 17)
†22 ms^{-1} obtained with adiabatic Lapse Rate
††Peak velocity at top of inversion for this run was 12 ms^{-1}

for the more stable cases in which evaporative cooling is less effective. This points to the importance of water loading.

Water loading for 50 dBZ is roughly 4 g kg^{-1} at cloud base. In conditionally neutral air this loading, acting between cloud base and the surface, could generate downdrafts of > 10 m s^{-1}. For 45 dBZ rain the loading is approximately 1.7 g kg^{-1}, which could generate downdrafts of > 5 m s^{-1}.

In general, the results obtained with this simplistic modeling approach are consistent with a hypothesis that precipitation loading and evaporative cooling may have been primary mechanisms for the microbursts.

8. CONCLUSIONS

Six microbursts and one microburst line which occurred near Denver, Colorado, on June 22, 1982, during the JAWS Project were examined by analysis of Doppler radar, rawinsonde, and surface network observations.

The microburst-producing storms apparently developed in response to interaction of wind parallel lines of convection and boundary-layer convergence lines. Initially a weak convergence line, possibly topographically induced, developed across the network. A gust front propagating from the south and a poorly defined surge from the northwest initiated further deep convection along the wind parallel lines and strengthened the existing convergence boundary.

Study of the life cycle of the microburst outflows revealed that the microbursts grew and strengthened from initial surface divergence, reaching maximum intensity several minutes later. Microburst structure fell into three categories: isolated microbursts in weak environmental flow with generally symmetric outflows; microbursts embedded in strong low-level flow with very asymmetric outflows; and the microburst line, consisting of several microbursts and exhibiting a quasi-linear divergence pattern. Some of the microbursts and the microburst line decayed simply by weakening, but two microbursts became larger-scale outflows.

Tentative conclusions may be drawn about the relative importance of proposed forcing mechanisms for these microbursts. All events occurred in descending heavy precipitation shafts. It follows that loading may be an important source of energy. Convergence into the area of downdraft within the dry layer just below cloud base, evidence of low-reflectivity notches in the neighborhood of the microburst downdrafts, and subsaturated surface conditions in the microburst outflows suggest active evaporation processes for these microbursts. Cold cloud base temperatures, high reflectivities indicative of the presence of graupel and hail, and indications of a radar bright band all suggest that melting may be important.

Calculations with a simple one-dimensional microphysical model confirm the intuitive reasoning that evaporation and precipitation loading contribute sufficient negative buoyancy to account for the magnitude of observed downdrafts. The results showed that with realistic lapse rates and precipitation rates, downdrafts sufficient to produce the microburst outflows could be generated. Melting, not included in the model, provides an additional source of negative buoyancy similar to evaporation.

33

Rotation is seen in most cases but its location with respect to the downdraft was variable. Timing of the appearance of rotation during the microburst life cycle varied from case to case and well-developed rotation seemed to be rather short-lived. These observations, and the separation of some of the microbursts from the convergence line, suggest that dynamic forces are not the primary cause of the strong downdrafts on this day.

It is concluded that the microbursts on June 22 were predominantly driven by microphysical and related thermodynamic effects due to precipitation loading and water phase change. Dynamic effects may be contributory in some cases but they do not appear to be of primary importance.

Surface network observations permitted identification of some, but not all, of the microbursts. Early detection of microbursts from surface observations also was not possible. Much smaller grid scale networks with much faster sampling times are necessary (Wilson and Flueck, 1986).

Descending cores such as those shown in Fig. 16 offer promise of very short-term warnings, but much work remains to be done (Roberts and Wilson, 1984, 1986). The descending reflectivity core first appears aloft before surface outflow is observed, but the maximum core does not usually occur at the surface until near the time of maximum outflow intensity.

Further modeling efforts with multi-dimensional models are needed to better define the physics of downdraft initiation and enhancement by evaporation, melting, and loading. Detailed simulations are required to identify conditions under which rotation can be expected to play a primary role in microburst forcing. Acquisition and analysis of multiple-Doppler wind fields and aircraft data extending well above cloud base for microburst cases in both dry and humid environments are critical to a proper understanding of microburst forcing mechanisms.

9. ACKNOWLEDGMENTS

REFERENCES

Abbs, D.J., and R.A. Pielke, 1986: Thermally forced surface flow and convergence patterns over northeast Colorado. *Mon. Wea. Rev.*, **114**, 2281-2296.

Bedard, A.J., Jr., and T.J. LeFebvre, 1986: Surface measurements of gust fronts and microbursts during the JAWS project: Statistical results and implications for wind shear detection, prediction, and modeling. *NOAA Tech. Memo. ERL WPL-135*, 112 pp.

Brock, F.V., and P.K. Govind, 1977: Portable Automated Mesonet in operations. *J. Appl. Meteor.*, **16**, 299-310.

Brown, J.M., K.R. Knupp, and F. Caracena, 1982: Destructive winds from shallow, high-based cumulonimbi. Preprints: 12th Conf. on Severe Local Storms. Amer. Meteor. Soc., Boston, Mass., 272-275.

Byers, H.R., and R.R. Braham, Jr., 1949: *The thunderstorm*. Government Printing Office, Washington, D.C., 287 pp.

Carbone, R.E., 1983: A severe frontal rainband. Part II: Tornado parent vortex circulation. *J. Atmos. Sci.*, **40**, 2639-2654.

Clark, T.L., and R. List, 1971: Dynamics of a falling particle zone. *J. Atmos. Sci.*, **28**, 718-727.

Cressman, G.P., 1959: An operational objective analysis scheme. *Mon. Wea. Rev.*, **87**, 367-381.

Elmore, K.L., J. McCarthy, W. Frost, and H.P. Chang, 1986: A high resolution spatial and temporal multiple Doppler analysis of a microburst and its application to aircraft flight simulation. *J. Clim. Appl. Meteor.*, **25**, 1398-1425.

Fujita, T.T., 1981: Tornadoes and downbursts in the context of generalized planetary scales. *J. Atmos. Sci.*, **38**, 1511-1534.

——, 1985: *The downburst*. Dept. of Geophysical Sci., Univ. of Chicago, Chicago, Ill., SMRP Rep. 210, 122 pp.

——, and H.R. Byers, 1977: Spearhead echo and downbursts in the crash of an airliner. *Mon. Wea. Rev.*, **105**, 129-146.

——, and R.M. Wakimoto, 1983: Microbursts in JAWS depicted by Doppler radars, PAM, and aerial photographs. Preprints: 21st Radar Meteor. Conf. Amer. Meteor. Soc., Boston, Mass., 638-645.

Hjelmfelt, M.R., and R.D. Roberts, 1985: Microburst lines. Preprints: 14 Conf. on Severe Local Storms. Amer. Meteor. Soc., Boston, Mass., 297-300.

Kamburova, P.L., and F.H. Ludlum, 1966: Rainfall evaporation in thunderstorm downdrafts. *Quart. J. Roy. Meteor. Soc.*, **92**, 510-518.

Kessinger, C.J., P.S. Ray, and C.E. Hane, 1983: An Oklahoma squall line: A multiscale observational and numerical study. CIMMS Report and Contribution No. 34, University of Oklahoma, Norman, Okla., 221 pp.

Klemp, J.B., and R. Rotunno, 1983: A study of the tornadic region within a supercell thunderstorm. *J. Atmos. Sci.*, **40**, 359-377.

Knupp, K.R., 1985: *Precipitating convective cloud downdraft structure: A synthesis of observations and modeling.* Ph.D. dissertation, Dept. of Atmos. Sci., Colorado State Univ., Ft. Collins, Colo., Atmos. Sci. Paper No. 387, 296 pp.

Kropfli, R.A., 1986: A microburst observed by high resolution dual-Doppler radar. Preprints: 23rd Conf. on Radar Meteor. Amer. Meteor. Soc., Boston, Mass., J109-J112.

McCarthy, J., R.D. Roberts, and W. Schreiber, 1983: JAWS data collection, analysis highlights, and microburst statistics. Preprints: 21st Radar Meteor. Conf. Amer. Meteor. Soc., Boston, Mass., 596-601.

———, J.W. Wilson, and T.T. Fujita, 1982: The Joint Airport Weather Studies project. *Bull. Amer. Meteor. Soc.*, **63**, 15-22.

Oye, R., and R.E. Carbone, 1981: Interactive Doppler editing software. Preprints: 20th Radar Meteor. Conf. Amer. Meteor. Soc., Boston, Mass., 683-687.

Pratte, J.F., and R.J. Clark, 1983: PROFS MESONET - Description and performance. Preprints: 5th Symp. on Meteor. Obs. and Instr., Amer. Meteor. Soc., Boston, Mass., 303-307.

Purdom, J.F.W., and K. Marcus, 1982: Thunderstorm trigger mechanisms over the southwest United States. Preprints: 12th Conf. on Severe Local Storms, San Antonio, Tex. Amer. Meteor. Soc., Boston, Mass., 487-488.

Rasmussen, R.M., V. Levizzani, and H.R. Pruppacher, 1984: A wind tunnel and theoretical study of the melting behavior of atmospheric ice particles III: Experiment and theory for spherical ice particles of radius > 500 m. *J. Atmos. Sci.*, **41**, 381-388.

Roberts, R.D., and J.W. Wilson, 1984: Precipitation and kinematic structure of microburst-producing storms. Preprints: 22nd Radar Meteor. Conf., Amer. Meteor. Soc., Boston, Mass., 71-76.

———, and J.W. Wilson, 1986: Nowcasting microburst events using single Doppler radar data. Preprints: 23rd Conf. on Radar Meteor., Amer. Meteor. Soc., Boston Mass., R14-R17.

Sekhon, R.S., and R.C. Srivastava, 1971: Doppler radar observations of drop-size distributions in a thunderstorm. *J. Atmos. Sci.*, **28**, 983-994.

Srivastava, R.C., 1985: A simple model of evaporatively driven downdraft: Application to microburst downdraft. *J. Atmos. Sci.*, **42**, 1004-1023.

Szoke, E.J., M.L. Weissman, T.W. Schlatter, F. Caracena, and J.M. Brown, 1984: A sub-synoptic analysis of the Denver tornadoes of 3 June 1981. *Mon. Wea. Rev.*, **112**, 790-808.

Wilson, F.W., Jr., and M.J. Carpenter, 1983: Portable Automated Mesonet: Real-time display capability. Preprints: 5th Symp. on Meteor. Obs. and Instr. Amer. Meteor. Soc., Boston, Mass., 321-325.

————, and J.A. Flueck, 1986: A study of the methodology of low-altitude wind shear detection with special emphasis on the Low-Level Wind Shear Alert System concept. Federal Aviation Administration report DOT/FAA/PM-86/4, 101 pp.

Wilson, J.W., 1986: Tornadogenesis by non-precipitation induced wind shears. *Mon. Wea. Rev.*, **114**, 270-284.

————, R.D. Roberts, C.J. Kessinger, and J. McCarthy, 1984: Microburst wind structure and evaluation of Doppler radar for airport wind shear detection. *J. Clim. and Appl. Meteor.*, **23**, 898-915.

————, and W.E. Schreiber, 1986: Initiation of convective storms at radar- observed boundary layer convergence lines. *Mon. Wea. Rev.*, **114**, 2516-2536.

END

10-81

DTIC